LTRPC2 Ca^{2+}-Permeable Channel Activated by Changes in Redox Status Confers Susceptibility to Cell Death

Yuji Hara

Doctor of Philosophy

Department of Physiological Sciences

School of Life Science

The Graduate University for Advanced Studies

2001 (School Year)

CONTENTS

INTRODUCTION

Changes in redox status induce necrotic/apoptotic processes in reperfusion injury during ischemia, degenerative diseases, and normal cellular functions (Coyle and Puttfarcken, 1993; Giroux and Scatton, 1996; Kietzmann et al., 2000). Regulation of intracellular Ca^{2+} concentration ($[Ca^{2+}]_i$) is also critical in both normal and pathological cellular processes (Choi, 1995; Mattson, 1996; Berridge et al., 1998). In acute insults such as hypoxia-ischemia, it has been proposed that the resultant cell fate (necrosis, apoptosis, or survival) is dependent on an intracellular 'Ca^{2+} setpoint' (Choi, 1995). Accumulating evidence indicates that cell injury, induced by disruption of redox state, is at least in part due to $[Ca^{2+}]_i$ dyshomeostasis, via production of bioactive molecules such as reactive oxygen species (ROS) and reactive nitrogen species (RNS) and their interaction with ion transport mechanisms (Kourie, 1998) including Ca^{2+} channels (Koliwad et al., 1996; Bielefeldt et al., 1997; Klonowski-Stumpe et al., 1997; Kourie, 1998; Lipton and Nicotera, 1998; Li et al., 1998; Mendez and Penner, 1998; Herson et al., 1999). However, the molecular entity of the Ca^{2+} channels activated specifically by modification of redox state is totally unknown. Furthermore, in nearly all cases to demonstrate this type of Ca^{2+}-permeable cation conductance, oxidants such as H_2O_2 at high concentrations 10 mM - 1 M, that would affect at the same time other Ca^{2+} transport mechanisms and ion channels (Kourie, 1998), have been employed (Li et al., 1998; Mendez and Penner, 1998; Herson et al., 1999). While some recent reports implied that ROS causes $[Ca^{2+}]_i$ elevations at much lower concentrations that do not

irreversibly damage the cells to lead to immediate death (Bielefeldt et al., 1997).

The *transient receptor potential* (*trp*) protein (TRP) superfamily consists of a diverse group of Ca^{2+}-permeable nonselective cation channels that bear structural similarities to *Drosophila* TRP (Montell and Rubin, 1989). *Drosophila* TRP comprises the light-activated, phosphatidylinositol (PI)-dependent Ca^{2+}-conductance in photoreceptor cells (Fasolato et al., 1994). TRP-related proteins play important roles in nonexcitable cells, as demonstrated by the recent finding that the mammalian homologue of TRP4 is expressed in endothelial cells and functions in vasorelaxation (Freichel et al., 2000). TRP superfamily contains a number of physiologically important Ca^{2+}-permeable cation channels such as capsaicin receptor (VR1), polycistin (PKD), osmolarity-sensing channel (OTRPC4), and Ca^{2+}-adsorption channel (ECaC) (Montell, 2001). 'Long' TRP (LTRP) family is one of the TRP superfamily. LTRP channels have a unique conserved amino-terminal region of 600-700 amino acid residues among the family, putative pore-forming transmembrane spans, and a C-terminal extension of variable length, and unique structures for individual LTRPC members (Harteneck et al., 2000). However, the channel activity or physiological function of LTRP family has been totally unknown.

I here report a novel redox status-dependent Ca^{2+}-permeable cation channel LTRPC2, whose intrinsic sensitivity to an activation trigger β-nicotinamide adenine dinucleotide (β-NAD^+) may underlie susceptibility of cells to death.

RESULTS

LTRPC2 mediates Ca^{2+} entry activated by micromolar H_2O_2

LTRPC2, originally reported as 'TRPC7' abundantly expressed in human brain (Nagamine et al., 1998), belongs to the 'LTRP' family together with other proteins such as melastatin (MLSN-1) (Hunter et al., 1998). cDNA for the human LTRPC2 (hLTRPC2) and its mouse homologue (mLTRPC2) were cloned from brain (Figure 1A). Sequencing analysis of the isolated mouse LTRPC2 cDNA clones revealed that the nucleotide sequence encodes a protein which shows 85% identity with the human LTRPC2.

A hydropathy profile reveals eight hydrophobic segments and the N and C hydrophilic termini (Figure 1B), similar to those of other TRP family. A phylogenetic tree reveals a gene superfamily for Ca^{2+}-permeable cation channels (Figure 2A). LTRPC2 shows 26% amino acid sequence identity with hMLSN-1, while LTRPC2 is distantly related with the classical TRP protein family comprising TRP1-7 (13% identity) and the vanilloid receptors and the osmo- and mechano-receptor channels (7-8% identity) (Harteneck et al., 2000; Inoue et al., 2001). Expression of LTRPC2 mRNA was widely distributed, being abundant in the lung, spleen, eye, and brain (Figure 2B).

Transient transfection of the hLTRPC2 and mLTRPC2 cDNAs elicited protein expression localized near the plasma membrane in HEK cells together with the transfection marker surface antigen CD8 (Figure 2C). Effects of H_2O_2 were examined in LTRPC2-expressing cells on $[Ca^{2+}]_i$ using fura-2. Surprisingly, 30 μM H_2O_2, which was

reported to be insufficient for immediate cell death (Bielefeldt et al., 1997), caused a prominent $[Ca^{2+}]_i$ increase within 20 min in 8 out of 66 CD8-positive LTRPC2-expressing cells. Elevation of the H_2O_2 concentration dramatically shortened the latency, prolonged responses, and increased the number of H_2O_2-responsive cells (Figure 2D): 10 mM H_2O_2 induced $[Ca^{2+}]_i$ rises in 92% of LTRPC2-expressing cells. Maximum $[Ca^{2+}]_i$ rises evoked in LTRPC2-expressing cells showed highly nonlinear dependence on the H_2O_2 concentration (Figure 2E).

By contrast, fewer number of TRP3- or TRP6-expressing cells displayed only small H_2O_2-iduced $[Ca^{2+}]_i$ rises nearly indistinguishable from those in vector-transfected control cells (Figure 2D and 2E). This excludes the possibility that the observed H_2O_2-induced $[Ca^{2+}]_i$ rises in LTRPC2-expressing cells are due to non-specific breakdown of cell membrane and consequent Ca^{2+} influx. It must be noted that TRP3, TRP6, and endogenous capacitative Ca^{2+} entry channels in HEK cells are capable of inducing $[Ca^{2+}]_i$ rises that reach nearly 600 nM in response to receptor stimulation or store depletion (Figure 6; Inoue et al., 2001).

The H_2O_2-induced $[Ca^{2+}]_i$ elevation was observed in LTRPC2-expressing cells only after the addition of Ca^{2+} to external solution (Figure 2F), and was suppressed to 43 ± 10% of control by 100 μM Ni^{2+}. H_2O_2-induced Mn^{2+} influx was markedly enhanced by LTRPC2 expression (Figure 3). These results demonstrate that LTRPC2 mediates Ca^{2+} influx in response to H_2O_2 of micromolar levels.

I examined the effects of other oxidants on LTRPC2. *tert*-butyl hydroperoxide (tBOOH) (≥0.035% = 4 mM), which only slightly increased $[Ca^{2+}]_i$ in control cells,

induced LTRPC2-mediated $[Ca^{2+}]_i$ elevation with a similar time course as H_2O_2 (Figure 4A). Application of 1 mM dithionite ($Na_2S_2O_4$), which generates superoxide anion (Archer et al., 1995), induced significantly higher $[Ca^{2+}]_i$ rises (1060 ± 608 nM) in LTRPC2-expressing cells, compared to those in control cells (44 ± 6 nM). I also examined whether LTRPC2 channels are activated by perturbation of endogenous levels of ROS (Figure 4B). Co-expression of the dominant negative mutant of thioredoxin (Ueno et al., 1999), known as a major intracellular antioxidant mechanism together with glutathione, induced LTRPC2-mediated $[Ca^{2+}]_i$ elevation in response to 10 μM H_2O_2, that by itself failed to evoke $[Ca^{2+}]_i$ elevation. Pretreatment with a catalase inhibitor 3-amino-1,2,4-triazole (ATZ) (1 mM), or a superoxide dismutase (SOD) inhibitor diethyldithiocarbamic acid (DETC) (1 mM) also elicited $[Ca^{2+}]_i$ rises via LTRPC2 in response to 10 μM H_2O_2. Previous publications have demonstrated both toxic (Buisson et al., 1992) and protective effects (Wink et al., 1993) of nitric oxide (NO) in ischemia/reperfusion. NO donor *S*-nitroso-*N*-acetyl-DL-penicillamine (SNAP) (300 μM) by itself induced small LTRPC2-mediated $[Ca^{2+}]_i$ elevation, and enhanced its H_2O_2 sensitivity to elicit $[Ca^{2+}]_i$ response to 10 μM H_2O_2 (Figure 4C). 1,2,3,4-oxatriazolium-5-amino-3-(3,4-dichlorophenyl)-chloride (GEA 3162) (100 μM) potently elevated $[Ca^{2+}]_i$ in LTRPC2-expressing cells, whereas the peroxynitrite donor 3-(4-morpholinyl) sydnonimine hydrochloride (SIN-1) (100 and 300 μM, and 1 mM) (Figure 4C) or NO donor 1-hydroxy-2-oxo-3-(3-aminopropyl)-3-isopropyl-1-triazene (NOC 5) (1 mM) was ineffective in inducing or potentiating $[Ca^{2+}]_i$ elevation (data not shown). Thus, ROS and RNS can activate LTRPC2, although some variability was

observed in potency among the RNS-generating agents.

Regulatory mechanisms of LTRPC2 activation

Amino acid oxidation modulates of various types of Ca^{2+} and K^+ channels (Ruppersberg et al., 1991; Chiamvimonvat et al., 1995; DiChiara and Reinhart, 1997; Li et al., 1998; Xu et al., 1998). However, coexpression of peptide methionine (Met) sulfoxide reductase (MsrA), known to accelerate inactivation kinetics of A-type K^+ channels (Kuschel et al., 1999), did not suppress LTRPC2-mediated Ca^{2+} increase induced by 1 mM H_2O_2 (100 ± 7%). The cysteine-specific oxidizing agent 2,2'-dithiobis (5-nitropyridine) (DTBNP) (50 μM) (Li et al., 1998) elicited similar $[Ca^{2+}]_i$ rises in control (144 ± 3 nM) and LTRPC2-expressing cells (139 ± 4 nM), suggesting that the $[Ca^{2+}]_i$ elevation induced by cysteine oxidation is an endogenous property of HEK cells. Supportively, the typical reducing agent DTT (1 mM), which can reverse amino acid oxidation, failed to suppress the H_2O_2-induced Ca^{2+} influx via LTRPC2 (98 ± 3%). The results suggest that activation of LTRPC2 occurs via the characteristic mechanisms distinct from amino acid oxidation.

Our experiments also revealed important modulatory factors for LTRPC2 channels. Arachidonic acid (AA) (30 μM) greatly potentiated Mn^{2+} influx in LTRPC2-expressing cells without H_2O_2, whereas it only slightly affected Mn^{2+} influx in control cells (Figure 5A and 5B). The responsiveness of LTRPC2 to AA was comparable to that of TRPL channels (Chyb et al., 1999). The AA-induced Mn^{2+} influx in LTRPC2-expressing cells was not inhibited by a lipoxygenase blocker nordihydroguaiaretic acid (NDGA) or a

cyclooxygenase blocker indomethacin (Figure 5C and 5D), suggesting that AA *per se* but not its metabolites is a positive regulator of LTRPC2. H_2O_2-induced Mn^{2+} influx via LTRPC2 was markedly enhanced by extracelluar Ca^{2+} (0.1 mM), that failed to affect Mn^{2+} influx in control cells (Figure 3A and 3B). This is indicative of a positive regulatory role of external Ca^{2+} in the LTRPC2 activation by H_2O_2, and contrasts to AA-induced LTRPC2 activation (Figure 5A). Ca^{2+} released from internal stores by AA in HEK cells (data not shown) may suffice LTRPC2 activation in the absence of external Ca^{2+}. Importantly, LTRPC2 did not potentiate $[Ca^{2+}]_i$ rises induced by stimulation of endogenous G protein-coupled muscarinic receptors (98 ± 8%) (Figure 6A and 6C) and ATP receptors (98 ± 7%), or by store depletion using thapsigargin (TG) (97 ± 7%) (Figure 6B and 6C) and cyclopiazonic acid (102 ± 10%), in contrast to TRP3, 5, 6, and 7 in HEK cells (Figure 6A; Inoue et al., 2001). Thus, LTRPC2 is a novel type of Ca^{2+}-permeable cation channel distinct in activation mechanism from receptor mediated- or store-operated channels.

Agonistic action of β-NAD^+ induces activation of LTRPC2 channel currents

To establish channel properties of LTRPC2, ionic currents were examined at a holding potential (V_h) of -50 mV in the nystatin-perforated patch recording (Figure 7A). In 26 out of 54 hLTRPC2-expressing cells, 100 μM H_2O_2 elicited inward currents comprised of three phases: the initial lag phase, the slowly developing second phase, and the third phase which rapidly reached the peak (117 ± 33 pA/pF). Time to reach the peak was 300 ± 23 s, which may imply gradual accumulation of a direct trigger of the LTRPC2

channel. In TRP3- and TRP6-expressing cells, 100 μM H_2O_2 elicited small inward currents (3 ± 1 and 5 ± 1 pA/pF, respectively) (n = 4), and no detectable currents in control cells (n = 17). The inward current was abolished by replacement of Na^+ with NMDG or by omission of external Ca^{2+} (Figure 7A and 7B), but was unaltered by reduction of the Cl^- concentration (data not shown). The results indicate that Na^+ is the main charge carrier of the LTRPC2 current, and are consistent with the importance of extracellular Ca^{2+} as a positive regulator for LTRPC2.

In contrast to the nystatin patch recordings, 100 μM H_2O_2 failed to evoke significant inward currents in the conventional whole-cell configuration (n = 55). This together with apparent lack of involvement of Met or Cys oxidation in LTRPC2 activation implicated that a cytoplasmic factor mediates for H_2O_2-evoked LTRPC2 activation. Recent publications demonstrate important roles of NAD^+ as a signaling molecule in physiological functions such as life span extension and monitoring of cellular energy and redox states (Lin et al., 2000; Ziegler, 2000). I presumed NAD^+ as a cytoplasmic activator for LTRPC2, since oxidized form NAD^+ could be generated by shift of the redox state to oxidizing by H_2O_2. In fact, using reverse phase high-performance liquid chromatography (HPLC), I observed an increase of NAD^+ content (from 1.43 ± 0.07 to 2.52 ± 0.18 nmole/mg protein, n = 4) (Figure 8A) and a decrease of NADH content (from 0.38 ± 0.02 to 0.14 ± 0.01 nmole/mg protein, n = 4) after 5 min exposure to 30 μM H_2O_2 in HEK cells (Figure 8B). Furthermore, I observed 25% decrease of NAD(P)H autofluorescence indicative of an increased $NAD(P)^+$/NAD(P)H ratio in HEK cells incubated with 100 μM H_2O_2 (400 s) (Figure 8C), as reported previously

(Herson et al., 1999; Tretter and Adam-Vizi, 2000). Compared to the oxidants H_2O_2 and tBOOH (0.35%) and the RNS-generating agents SNAP and GEA 3162, that effectively activated LTRPC2 (Figure 4C), SIN-1 and NOC 5 that failed to activate LTRPC2 (Figure 4C) elicited significantly smaller autofluorescence decrease (Figure 8C). Thus, the increase in $NAD(P)^+$/NAD(P)H ratio correlates well with the potency of the ROS- and RNS-generating agents to evoke LTRPC2 activation.

When hLTRPC2-expressing cells were dialyzed with a patch pipette solution containing 1 mM β-NAD^+, inward currents gradually developed and reached peak in 9 - 13 min in 24 out of 124 cells (321 ± 117 pA/pF; maximal response, 1241 pA/pF) (Figure 9A), whereas only 2 out of 14 control cells showed tiny inward currents (2 and 18 pA/pF). A dose-response curve relating β-NAD^+ concentration to the current density demonstrated that LTRPC2 was not activated by β-NAD^+ of $\leq$500 μM, but that nearly maximal current amplitude was attained by 3 mM β-NAD^+ and 100% response by 5 mM β-NAD^+ (Figure 9C). The β-NAD^+-induced LTRPC2 currents were also markedly reduced by omission of extracellular Ca^{2+} or by replacement of Na^+ with NMDG (Figure 9A), which excludes a possibility that non-specific leak currents were evoked by β-NAD^+. The I-V curve of β-NAD^+-induced LTRPC2 currents was linear with a reversal potential of +2.7 ± 0.8 mV (n = 14) (Figure 9B), being similar to that of H_2O_2-induced LTRPC2 currents with a reversal potential of -2.7 ± 1.4 mV (n = 6) (Figure 7B). Other β-NAD^+-related molecules such as NADH (1 mM), $NADP^+$ (3 mM), and cADP ribose (20 μM) failed to activate the LTRPC2 channel. In addition, other physiological cellular components, NADH (50 μM), $NADP^+$ (70 μM), NADPH (50

μM), ADP (800 μM), and ATP (2 mM) (Dunne et al., 1988) in the pipette did not affect the LTRPC2 activity evoked by 1 mM β-NAD^+, while they slightly lowered the threshold for LTRPC2 activation to elicit small LTRPC2 currents in response to 500 μM β-NAD^+ (7.7 ± 1.1 pA/pF) (n = 4) (Figure 9C). Three mM β-NAD^+ with 10 mM BAPTA in the pipette solution evoked no significant inward LTRPC2 currents. Since $[Ca^{2+}]_i$ elevation by TG or receptor stimulation failed to activate LTRPC2 (Figure 6) (data not shown), the result suggests that Ca^{2+} is necessary but is not sufficient for LTRPC2 activation. Furthermore, extracellular application of 10 μM AA shifted dependence of LTRPC2 currents on β-NAD^+ toward lower concentrations and suppressed maximal LTRPC2 current amplitudes (Figure 9C), revealing an interesting modulatory effect of AA that enhances β-NAD^+ sensitivity of LTRPC2.

Direct interaction of β-NAD^+ with MutT motif is critical for LTRPC2 activation

Structural comparison of LTRPC2 with other proteins revealed an amino acid sequence homologous to the 'MutT' module, conserved among the active sites of nucleoside diphosphate hydrolyzing enzymes (Bessman et al., 1996), in the putatively cytoplasmic C-terminal region (Figure 10A). The LTRPC2 construct with a deletion of the MutT sequence showed no detectable Ca^{2+} influx activity in response to H_2O_2 up to 30 mM (Figure 10C) and slightly but significantly reduced Mn^{2+} influx activity in response to AA (Figure 10D). Since replacing the Met residue (M1397) with isoleucine in the MutT motif (M1397I) only slightly affected the LTRPC2 activity, oxidation of M1397 is not an absolute requirement for LTRPC2 activation. In the putatively cytoplasmic

N-terminus, I also found the sequence that resembles the charged region responsible for the stimulation of the two-pore domain TREK-1 K^+ channel by AA (Figure 10B) (Patel et al., 1998). Deletion of the motif (AA-responsive sequence (ARS)) abrogated responsiveness of LTRPC2 to both AA and H_2O_2 (Figure 10C and 10D). The deletion mutants elicited no significant inward currents in cells dialyzed with 3 or 30 mM β-NAD^+ despite localization near the plasma membrane (Figure 11: compare wild-type in Figure 2C). Thus, MutT and ARS are critical structural bases for β-NAD^+- and AA-dependent activation of LTRPC2 channels.

Two additional experiments supported direct interaction of β-NAD^+ with the LTRPC2 protein. Firstly, inward currents were immediately induced by β-NAD^+ applied from the cytoplasmic side of inside-out membrane patches excised from hLTRPC2-expressing cells (Figure 12A). After omission of β-NAD^+, the activity sustained but gradually diminished, and unitary opening events became resolvable (Figure 12A). By contrast, no similar unitary activity was observed in the excised patches from control cells (n = 20). Unitary LTRPC2 currents were also recorded from a cell-attached patch in H_2O_2-treated LTRPC2-expressing cells (Figure 12B). When the patch was pulled off and excised as a inside-out patch, the activity disappeared, but was restored by application of 3 mM β-NAD^+ instead of H_2O_2 (Figure 12C). The H_2O_2-induced and β-NAD^+-activated unitary activities showed similar long openings and linear I-V relationships, reminiscent of those of whole-cell currents (Figure 12Da and 12Db). The unitary conductance of the H_2O_2-induced channel (52.3 ± 2.8 pS) and that of the β-NAD^+-activated channel (59.0 ± 1.3 pS) showed no statistically significant

difference. Omission of Ca^{2+} from the solution perfused on inside-patches using 10 mM BAPTA abolished the β-NAD^+-induced activity, leading to an idea that extracellular Ca^{2+} required for activation passes through the LTRPC2 channel to act from the intracellular side. The results strongly suggest the identity of the β-NAD^+-activated channel with the H_2O_2-activated channel in LTRPC2-expressing cells. Secondly, biochemical experiments demonstrated direct interaction of β-NAD^+ with LTRPC2 (Figure 13). ^{32}P-labeled β-NAD^+ showed potent binding to the GST fusion protein of the hLTRPC2 C-terminus, but much weaker binding to the fusion protein with the MutT deletion, suggesting a secondary interaction between chemical groups other than nucleotide diphosphate of β-NAD^+ with a LTRPC2 structure outside MutT. The results altogether supports that direct action of β-NAD^+ to the MutT motif mediates activation of the Ca^{2+}- and Na^+-permeable cation channel LTRPC2.

Heterologous LTRPC2 expression confers susceptibility to H_2O_2-induced cell death

LTRPC2-expressing cells were significantly susceptible to cell death induced by exposure to H_2O_2 (≥10 μM) in trypan blue exclusion assay (Figure 14A), and to reduction of cell survival by H_2O_2 (≥50 μM) in mitochondrial dehydrogenase activity assay (Figure 14C). In 4 out of 44 hLTRPC2-expressing cells, which showed $[Ca^{2+}]_i$ elevation, cell death assessed by propidium iodide (PI) staining was simultaneously observed after 30 min exposure to 100 μM H_2O_2 (Figure 14D), but $[Ca^{2+}]_i$ response or death was undetectable in control cells. By contrast, LTRPC2 in Ca^{2+}-free external solution, or the MutT- and ARS-deleted mutants, TRP3 or TRP6 conferred on HEK

cells only marginal susceptibility, if at all, to the impairment of trypan blue exclusion by H_2O_2 (≥1 mM) (Figure 14A and 14B), and elicited smaller reduction in viability induced by H_2O_2 (≥300 μM) (Figure 14C). In support of direct correlation between $[Ca^{2+}]_i$ elevation and cell death, H_2O_2 applied with 10 μM BAPTA-AM failed to induce cell death (Figure 14B). Cytoplasmic budding was observed in 68% of LTRPC2-expressing cells treated with 100 μM H_2O_2 (Figure 14E and 14F), whereas majority of the TRP3- and TRP6-expressing cells, and control cells were free from the prominent morphological change, except for 72% of the TRP3-expressing cells treated with 10 mM H_2O_2 (Figure 14F). It must be noted that 20 min stimulation of TRP3- and TRP6-expressing cells with 30 μM carbachol did not impair trypan blue exclusion, and that TRP3, TRP6, and LTRPC2 showed similar expression levels (3.8, 4.1, and 2.9 pmole/1x10^5cells for mTRP3, mTRP6, and hLTRPC2, respectively) and plasma membrane localization (Figure 15). Furthermore, activation of caspase-3 and DNA laddering were not induced in hLTRPC2-expressing cells by 100 or 300 μM H_2O_2. Thus, heterologous LTRPC2 channels are capable of mediating H_2O_2-induced cell death, which may be necrotic or caspase-independent

Ca^{2+} influx and cell death mediated by LTRPC2 in native systems

To investigate physiological functions of LTRPC2 channels in "native" systems, LTRPC2 expression was suppressed by treatment with the antisense oligonucleotide (Figure 16A and 16B). In rat insulinoma RIN-5F cells (Herson et al., 1997a, 1997b, 1999), the antisense oligonucleotide, which dramatically diminished LTRPC2

immunoreactivity localized near the plasma membrane and in the cytoplasmic area (Figure 16B), significantly suppressed Ca^{2+} influx (Figure 16C) and cell death (Figure 16D) induced by H_2O_2, in clear contrast with the sense oligonucleotide. It was found that ROS is generated downstream of tumor necrosis factor α (TNFα)-induced pathway (Gotoh and Cooper 1998). TNFα evoked $[Ca^{2+}]_i$ oscillation in RIN-5F cells (Figure 17). LTRPC2 antisense almost abolished this $[Ca^{2+}]_i$ response as observed for omission of extracellular Ca^{2+} (Figure 17). Strikingly, the antisense treatment significantly suppressed TNFα-induced death in RIN-5F cells (Figure 18A). Suppression of TNFα-induced death was achieved also in the presence of intracellular Ca^{2+} chelator BAPTA-AM and antioxidant glutathione, consistent with the critical role of Ca^{2+} and ROS in LTRPC2-mediated death. TNFα- and H_2O_2-induced cell death was similarly suppressed by the antisense treatment in the monocyte cell line U937 (Figure 18B). The results suggest important involvement of LTRPC2 in formation of "native" H_2O_2-activated Ca^{2+} channels that mediates cell death.

DISCUSSION

The present investigation reveals that LTRPC2 is the molecular entity of Ca^{2+}- and Na^+-permeable cation channel activated via agonistic binding of β-NAD^+ in response to changes in redox status (Figure 12). The present measurement of the cellular NAD^+ level and the previous estimation of the basal NAD^+ concentration ranging 200-350 μM (Dunne et al., 1988) suggest that the NAD^+ concentration elevated by H_2O_2 to the threshold near 500 μM mediates LTRPC2 activation. In fact, potency of oxidants and RNS-generating agents to activate LTRPC2 channels shows good correlation with their ability to increase the $NAD(P)^+$/NAD(P)H ratio. However, it is also possible that NAD^+ as an allosteric effector enhances the agonistic action of other factors such as AA. Since the effect of H_2O_2 on LTRPC2 was observed only in the electrophysiological techniques that retains the intracellular structure and composition, it is unlikely that direct action of ROS, protein modification, or membrane peroxidation by itself is sufficient for LTRPC2 activation, although basal oxidation at a redox site in LTRPC2, not reached by extracellularly applied DTT, can be involved in the activation. The results also indicate impairments of AA and H_2O_2 sensitivity by deletion of ARS in LTRPC2 channels, suggesting that AA is essential for β-NAD^+-dependent activation of LTRPC2. Endogenous AA may keep the activation threshold of LTRPC2 channel within a range of intracellular β-NAD^+ concentration H_2O_2 elevates, and exogenous AA may shift the threshold toward lower β-NAD^+ concentrations to facilitate current activation. Since H_2O_2 treatment has been reported to produce AA (Barlow et al., 2000), the β-NAD^+

concentration dependence lowered by AA may be involved in H_2O_2-induced LTRPC2 activation. Thus, LTRPC2 should be functionally categorized in a novel group of Ca^{2+} channels, distinct from STRPs and OTRPs (Harteneck et al., 2000). Two other papers on LTRPC2 appeared (Perraud et al., 2001; Sano et al., 2001). Our data is consistent with the papers in most functional aspects including linear I-V curves and activation triggers, except for the lack of inhibition by internal ATP, which may be due to our combining ATP with other physiological components (Figure 9).

Antisense experiments suggest an involvement of LTRPC2 in native H_2O_2-induced Ca^{2+} influx and cell death. Herson et al. (1997a, 1997b, and 1999) previously reported a β-NAD^+-activated non-selective cation (NS_{NAD}) channel induced by H_2O_2 in CRI-G1 rat insulinoma cells. The immediate and complete cessation of H_2O_2-induced NS_{NAD} channel activity by patch excision, linear I-V relationships, and lack of selectivity among cations are similar to what we observed for LTRPC2, suggesting that the NS_{NAD} channel represents the "native" LTRPC2 channel. Higher H_2O_2 and Ca^{2+} requirements of NS_{NAD} channels compared with those of LTRPC2 may be attributable to multimerization of LTRPC2 with other subunits or intracellular modulatory components in native systems. Non-selective cation channels activated under UV irradiation and oxidant stress by H_2O_2 and tBOOH of relatively high concentrations or by oxidized glutathione have been reported in various mammalian cells (Koliwad et al., 1996; Mendez and Penner, 1998). Since these cation channels survive in excised inside-out patches, they would be activated via a membrane-delimited pathway (Mendez and Penner, 1998) and may rather represent native counterparts of TRP3 and TRP6.

LTRPC2, that efficiently transforms changes in redox status to Ca^{2+} overload, is of great patho-physiological importance, since it enables the cell injury to directly affect and shift the intracellular 'Ca^{2+} setpoint', on which the resultant fate of the cell depends (Choi, 1995; Lipton and Nicotera, 1998). The results also indicate that LTRPC2 conducts a large amount of Na^{+}, which in combination with oxidative stress is important in the neuronal injury (Friedman and Haddad, 1993; Mattson, 1996). These features and wide tissue distribution suggest general significance of LTRPC2 in cell death and degenerative diseases. Since far less sensitivity to H_2O_2-induced death was conferred by TRP3 and TRP6 in the presence of extracellular Ca^{2+} or by LTRPC2 in the absence of Ca^{2+} (Figure 14), it is improbable that LTRPC2-mediated cell death is due to non-specific effects of membrane depolarization by overexpressed Ca^{2+}-permeable cation channels. The LTRPC2-mediated mechanism is different from non-specific disruption of the cell membrane integrity through lipid peroxidation, or even from Ca^{2+}-permeable cation currents induced by UV or oxidizing agents (Mendez and Penner, 1998), as discussed above. The mechanism is also distinct from the hypothesis that ROS causes DNA strand breaks, activation of nuclear poly (ADP-ribose) polymerase, and depletion of β-NAD^{+}, leading to cell death (Okamoto, 1985). Importantly, cell death in HEK cells mediated by LTRPC2 was not accompanied by DNA fragmentation or activation of caspase-3. This is unlikely to derive from the transient nature of our expression system, since transfection efficiency exceeding 20% should allow detection of DNA laddering. An alternative possibility that HEK cells are intrinsically insusceptible to apoptosis can be also excluded, since DNA fragmentation was induced

in HEK cells by staurosporine (unpublished data). Thus, the form of LTRPC2-mediated cell death may be necrotic or caspase-independent. Vercammen et al (1998a, 1998b) reported that there are two different pathways from Fas receptors in L929 fibrosarcoma cells, one rapidly leading to apoptosis, and a second directing the cells to necrotic cell death. Furthermore, as in TNFα-induced necrosis, Fas treatment led to accumulation of reactive oxygen species, and Fas-mediated necrosis was inhibited by the oxygen radical scavengers. It is necessary to elucidate whether LTRPC2 participates in the Fas-mediated necrotic pathway, as well as the physiological significance of Fas-induced necrotic cell death.

Recently, among the LTRP family, the activation mechanism of LTRPC7 was identified (Runnels et al., 2001; Nadler et al., 2001). LTRPC7 is ATP-dependent Ca^{2+}-permeable cation channel. LTRPC7 contains a putative kinase motif, and its kinase activity is necessary for channel function. It is proposed that LTRPC7, by virtue of its sensitivity to physiological Mg-ATP levels, may involved in a fundamental process that adjusts plasma membrane divalent cation fluxes according to the metabolic state of the cell. Furthermore, LTRPC7 may represent a direct mediator of the toxic divalent cation entry that occurs during severe metabolic stress conditions such as hypoxia or hypoglycaemia. LTRP channels may be 'determinants of cell fate' by sensing intracellular metabolic status. The LTRPC2 knockout mice will assist further studies of the LTRP channels.

EXPERIMENTAL PROCEDURES

Molecular cloning

To isolate the mouse homologue of LTRPC2 (mLTRPC2), a mouse brain cDNA library was screened with the hLTRPC2 (TRPC7) (Nagamine et al., (1998); AB001535) cDNA probes (hLTRPC2-5, hLTRPC2-6), obtained by PCR amplification from the human whole brain cDNA (CLONTECH) using the Marathon cDNA Amplification Kit (CLONTECH). The specific oligonucleotide primers used were as follows: hC1-5 (5'-CGGGGTGGAGATTCCTCTGAGGACCAGGCT-3') and hC1-12 (5'-GCCTTCTTCATCAGCCCGCACTCGTCAGGG-3') for hLTRPC2-5 (nucleotide residues 914-2579, numbered from the first residue of the ATG initiation triplet); hC1-7 (5'-TTTCCTCTGCCTGTTCGCCTACGTGCTCATG-3') and hC1-14 (5'-AGAGGGAGCTTCACCACCAGCACTTCCAGC-3') for hLTRPC2-6 (2425-4142). Screening of the oligo(dT)-primed, size selected (>1 kb) adult mouse (BALB/c) brain cDNA library constructed in the Uni-ZAP XR vector (Stratagene) using the hLTRPC2-6 probes yielded clone λmLTRPC2-9 (2781-5331). To obtain the entire coding sequence of the mLTRPC2 cDNA, rapid amplification of 5'-cDNA ends (5'-RACE) was performed using the template cDNAs constructed from C57BL/6J mouse brain poly(A)$^+$ RNA, and the Marathon cDNA Amplification kit (CLONTECH). The specific primers mC1-14 (5'-GGTGTAGTTGAACATGGCGATGAGCAGG-3') and mC1-13 (5'-CCAGTCGCTCTCAGGACACTTAGGCTTG-3') were used in first and nested PCR, respectively, to isolate the cDNA, mLTRPC2-2 (1076-3266). Another 5'-RACE

was carried using the specific primers mC1-12 (5'-CACATCCACATCCTGCTGACCATCC-3') and mC1-10 (5'-GCTTCTGCTGGATCAAGGAGATGG-3') in first and nested PCR to yield a cDNA fragment, mLTRPC2-1 (-236-1144). The cDNA fragments, mLTRPC2-1 and mLTRPC2-2, were subcloned into pGEM-T Easy vector (Promega) to yield clone pmLTRPC2-2 and pmLTRPC2-1.

Human LTRPC2 cDNA was isolated by PCR from human whole brain cDNA (CLONTECH) using the pairs of oligonucleotide primers as follows: hC1-1 (5'-GTGCATCTGCACCCGTGGGGGAGGGAGCTC-3') and hC1-10 (5'-TTGGCCACCTGGGCAATGACGTCGGCCACG) for hLTRPC2-1 (-367-1103); hC1-40(5'-AAAAGTACGTCCGAGTCT-3') and hC1-49 (5'-CAATGGCCCAAATGAGAAGGTCACG-3') for hLTRPC2-2 (419-1893); hC1-48 (5'-GGATGGTCAGCAGGACGTGGATGTG-3') and hC1-50 (5'-GATGGTGAGGTAGGAGTGGTAGACG-3') for hLTRPC2-3 (1269-2934); hC1-7 and hC1-18(5'-AAGCCCTGGTTTCTGGGGGGAACGTCTATG-3') for hLTRPC2-4 (2425-4570). The resulting PCR fragments using *pfu* DNA polymerase (Stratagene) were subcloned into *Eco*RV site of pBluescript II SK(+) (Stratagene) to yield phLTRPC2-1, phLTRPC2-2, phLTRPC2-3, and phLTRPC2-4.

To isolate hMsrA cDNA, PCR amplification from human whole brain cDNA was carried out using *TaKaRa LA Taq*™ with GC Buffer (Takara) and a pairs of oligonucleotide primers A2 (5'-GGTTTGGGCAACCTCGATTACGGGC-3') and A3 (5'-TTATCAACTTGCCATCGCGCCTCC-3').

Northern blot analysis of mLTRPC2

RNA blot hybridization analysis was carried out using total RNA (20 μg) from various tissues of 2-month-old C57BL/6J mice. The probe used to detect LTRPC2 RNA was the *Eco*RI fragment from pmLTRPC2-2 (1076-3266). Random Primer DNA Labeling Kit ver. 2 (Takara) was used to ^{32}P label the probe. Hybridization was performed at 42 °C in 50% formamide, 5×SSC, 50 mM sodium phosphate buffer (pH 7.0), 0.1% SDS, 0.1% polyvinylpyrrolidone, 0.1% Ficoll 400 (Amersham Pharmacia Biotech), 0.1% bovine serum albumin, and 0.1 mg/ml sonicated herring sperm DNA, as described previously (Okada et al., 1998).

Expression vectors

The expression plasmid for hLTRPC2 was constructed as follows. The PCR product (hLTRPC2-7) was amplified from hLTRPC2-1 cDNA using a sense primer (5'-AAGAATTCGGGTTTTTATTTTTAATTTTCTTTCAAATACTTCCACCATGGAG CCCTCAGCCCTG-3'), designed to contain the untranslated leader sequence from the alfalfa mosaic virus (Jobling and Gehrke, 1987), a consensus sequence for translation initiation (Kozak, 1986), and nucleotide residues 1-18 of human LTRPC2, and the antisense primer hC1-10. The 0.56-kb *Eco*RI (-43)/*Bst*EII (516) fragment from hLTRPC2-7, the 1.1-kb *Bst*EII (517)/*Bam*HI (1626) fragment from hLTRPC2-2, the 1.2-kb *Bam*HI (1627)/*Apa*I (2765) fragment from hLTRPC2-3, and the 1.8-kb *Apa*I (2766)/*Sal*I (on vector) fragment from hLTRPC2-4 were ligated with the 5.5-kb

*Eco*RI/*Sal*I fragment from pCI-neo (Promega) to yield pCI-neo-hLTRPC2. The expression plasmid for mouse LTRPC2 was constructed as follows. The PCR product obtained using the PCR cDNA fragment mLTRPC2-1 and the plasmid pmLTRPC2-2 with a pair of primers mC1-24 (5'AAGAATTCGGGTTTTTATTTTTAATTTTCTTTCAAATACTTCCACCATGGAG TCCTTGGACCGG-3') and mC1-27 (5'-ACGTCCAGTTTGTTCCAG-3'), and the PCR product obtained by using the PCR cDNA fragment mROSC-2 and the plasmid pmLTRPC2-3 with a pair of primers (5'-CCCAGAAGCTGCTTGTCC-3') and mC1-3' (5'-GAAGGTCGACTCAGAAGTGAGCTCCAAAC-3') were subcloned into the *Eco*RV site of pBluescript II SK(+) to yield the plasmids pmLTRPC2-4 and pmLTRPC2-5, respectively. The 2.3-kb *Eco*RI/*Sph*I fragment from pmLTRPC2-4 and the 2.2-kb *Sph*I/*Sal*I fragment were ligated with the 5.5-kb *Eco*RI/*Sal*I fragment from pCI-neo to yield pCI-neo-mLTRPC2.

Deletion and single amino acid substitution mutants were constructed using PCR techniques. Primers used for the mutagenesis were as follows: 5'-TGGGCCCTGCCTGGGCACTGGCCGTCTTTTG-3' and AAAAGACGGCCAGTGCCCAGGCAGGGCCCAG-3' for ΔMutT; 5'-AGGCTGGAGAGAGGAGGTGTGGCCATCAAG-3' and 5'-ACACCTCCTCTCTCCAGCCTGGTCCTCAGAG-3' for ΔARS; 5'-TCCCGGGAGCCAGGGGAGATACTACCTCGG-3' and 5'-CCGCTTCAGCTTCCGAGGTAGTATCTCCCCTG-3' for M1397I.

Cell cultures and recombinant expression in HEK293 cells

HEK293 (American Type Culture Collection) cells were cultured in Dulbecco's modified Eagle's medium (DMEM) containing 10% fetal bovine serum, 30 units/ml penicillin, and 30 μg/ml streptomycin. HEK293 cells were co-transfected with πH3-CD8 containing the cDNA of the T-cell antigen CD8 (Jurman et al., 1994) and one of pCI-neo-mLTRPC2, pCI-neo-hLTRPC2, pCI-neo-mTRP3, pCI-neo-mTRP6 (Inoue et al., 2001), and the vector pCI-neo. Transfection was carried out using SuperFect Transfection Reagent (Qiagen). Cells were trypsinized and diluted with DMEM and plated onto glass coverslips 24 h after transfection. Then cells were subjected to measurements 8-36 h after plating on the coverslips. LTRPC2-expressing cells were selected through detection of CD8 co-expression using polystyrene microspheres precoated with antibody to CD8 (Dynabeads M-450 CD8; Dynal). For co-expression of hMsrA (Kuschel et al., 1999) and the dominant negative mutant of thioredoxin (Ueno et al., 1999), equal amount of each expression plasmid was co-transfected to HEK cells.

Immunofluorescence staining

Anti-mouse LTRPC2 rabbit antiserum (mLTRPC2-C1) was raised against the C-terminus 1488-1506 (YANHKTILQKVASLFGAHF). Rabbit antisera to mouse TRP3 (mTRP3-C1) and mouse TRP6 (mTRP6-C1) (Inoue et al., 2001) were raised against the residues 771-792 (EELAILIHKLSEKLNPSVLRCE) and 736-755 (LIRKLGERLSLEPKLEESRR), respectively. Cells on coverslips were fixed with 4% (v/v) formaldehyde in phosphate-buffered saline (PBS) for 20 min at room temperature,

washed with PBS for three times, and then permeabilized with 0.2% (v/v) Triton X-100 in PBS for 10 min at room temperature. After wash in PBS for three times, the coverslips were incubated with 10% normal goat serum (NGS) for 1 h at room temperature. The cells were then incubated for 1 h at room temperature with polyclonal antibodies, diluted in 1% NGS in PBS, and incubated for 1 h incubation with the FITC-conjugated anti-rabbit IgG. The coverslips were sealed with PermaFluor Aqueous (IMMUNON^{TM}, Shandon) to prevent evaporation and stored at 4°C before imaging. The fluorescence images were acquired with a confocal laser scanning microscope (LSM 510, Zeiss) equipped with a krypton/argon ion laser. A single wavelength of 488 nm was used for excitation, and the emitted fluorescence at 505 nm was collected through an objective lens with a 63 or 86 times magnification (Plan Apochromat), and an optical section of 0.8 - 1.1 μm was projected on a single plane.

Fluorescent measurements of $[Ca^{2+}]_i$ changes and Mn^{2+} influx

Cells on coverslips were loaded with fura-2 by incubation in DMEM containing 1 μM fura-2/AM (Dojindo) and 10% fetal bovine serum at 37°C for 40 min. Then fura-2-loaded cells were incubated with DMEM containing Dynabeads M-450 CD8 for 5 min and washed with HEPES-buffered saline (HBS) containing (in mM) 107 NaCl, 6 KCl, 1.2 $MgSO_4$, 2 $CaCl_2$, 11.5 glucose, 20 HEPES, adjusted to pH 7.4 with NaOH. The coverslips were then placed in a perfusion chamber mounted on the stage of the microscope. Fluorescence images of the cells were recorded and analyzed with a video images analysis system (ARGUS-20/CA, Hamamatsu Photonics). The fura-2

fluorescence at an emission wavelength of 510 nm (bandwidth, 20 nm) was obtained at room temperature by exciting fura-2 alternately at 340 and 380 nm (bandwidth, 11 nm). The 340:380 nm ratio images were converted to Ca^{2+} concentrations by *in vivo* calibration (Nishida et al., 1999) using 5 μM ionomycin. All the reagents dissolved in water, ethanol, or dimethyl sulfoxide were diluted to their final concentrations in HBS or Ca^{2+}-free HBS containing (in mM) 107 NaCl, 6 KCl, 1.2 $MgSO_4$, 0.5 EGTA, 11.5 glucose, 20 HEPES, adjusted to pH 7.4 with NaOH, and applied to the cells by perfusion.

Mn^{2+} entry was measured through monitoring the decline of fluorescence of fura-2 induced by binding of Mn^{2+}. Fluorescence quenching was studied using the fura-2 isosbestic excitation wavelength of 360 nm and recording emitted fluorescence at 510 nm. The system used was the same as in the $[Ca^{2+}]_i$ measurement. The fluorescence intensity relative to the initial values were obtained on a pixel by pixel basis. $MnCl_2$, H_2O_2, and AA (Sigma, A8798, Lot 18H52131) were diluted to their final concentrations in nominally Ca^{2+}-free HBS. Rates for initial phase of reduction of fluorescent intensity were determined as described in Trepakova et al. (1999).

NAD(P)H autofluorescence of HEK cells was observed using excitation at 360 nm and emission at 460 nm (Eng et al., 1989).

Electrophysiology

Whole-cell currents were recorded at room temperature using the nystatin perforated-patch technique (Horn and Marty, 1988) or the conventional whole-cell

configuration (Hamill et al., 1981) with an Axopatch 200B amplifier (Axon Instruments). Currents were sampled at 200 Hz for Figure 7A and 9A, and at 1 kHz after low-pass filtered at 1 kHz (-3dB) using an 8-pole Bessle filter (900, Frequency Devices) for Figure 7B, 9D and 12A, and analyzed with pCLAMP 6.02 software (Axon Instruments). Patch pipettes were made from borosilicate glass capillaries (1.5 mm outer diameter; Hilgenberg) using a model P-97 Flaming-Brown micropipette puller (Sutter Instrument). Pipette resistance ranged from 2 to 4 MΩ when filled with the pipette solution described below. A stock solution containing 5 mg/ml nystatin was prepared and was added at a final concentration of 0.25 mg/ml to the pipette solution. whose composition was (mM): CsCl 150, $MgCl_2$ 2, EGTA 5, HEPES 5, adjusted to pH 7.2 with CsOH. The '0 mM Ca^{2+}-NaCl solution' contained (in mM): NaCl 121.7, $MgCl_2$ 1.2, $CaCl_2$ 1.2, EGTA 2, glucose 10, HEPES 11.5, mannitol 51, adjusted to pH 7.4 with NaOH (90 nM calculated free Ca^{2+}). The '2 mM Ca^{2+}-NaCl solution' contained (in mM): NaCl 125, $MgCl_2$ 1.2, $CaCl_2$ 2, glucose 10, HEPES 11.5, mannitol 51, adjusted to pH 7.4 with NaOH. The '2 mM Ca^{2+}-NMDG solution' was made by the substitution of equimolar NMDG-Cl for NaCl. For the inside-out and cell-attached patch recordings, the recording pipette contained the '2 mM Ca^{2+}-NaCl solution', and the bathing solution contained (mM): KCl 155, $CaCl_2$ 0.581, $MgCl_2$ 2, EGTA 2, HEPES 5, adjusted to pH 7.25 with KOH (50 nM calculated free Ca^{2+}). The resistance of silicone (KE106, Shin-Etsu Chemical) -coated and fire-polished pipettes was 4-8 MΩ. The osmolarity of every solution was adjusted to about 320 mOsm. Rapid change of external solutions was made by a modified "Y-tube" method (Wakamori et al., 1993). Data were

represented by the mean ± S.E..

Analysis of pyridine dinucleotide in HEK cells by HPLC

NAD^+ and NADH contents were measured using reversed-phase HPLC with a modification by Litt et al. (1989). For determination of NAD^+ and NADH, a 500 µl aliquot from the 2 ml cell suspension of a 10 cm dish culture was treated with 50 µl of 3 M perchloric acid and 0.5 M NaOH/50% (v/v) ethanol/35% CsCl, respectively. After 10 min centrifugation at 15,000 rpm, supernatants were separated on a TSK-Gel ODS-80Ts (4.6 x 250 mm) column (Tosoh). The mobile phase was 0.1 M KH_2PO_4 (pH 6.0)/5% methanol. NAD^+ and NADH were identified by UV detection (254 nm) and fluorometric detection (Ex. 370 nm, Em. 460 nm), respectively. Protein contents were determined by *Dc* Protein Assay Kit (Bio-Rad).

β-NAD^+ binding assay

The C-terminal regions of wild-type (amino acid residues 1,286-1,503) and the mutant hLTRPC2 (with deletion of the MutT motif, 1,390-1,409: ΔMutT) were inserted in *Eco*RI and *Sal*I site of pGEX-4T-3 (Pharmacia). Total proteins from *E.coli* (BL-21) expressing GST fusion proteins (GST-hLTRPC2-C or GST-ΔMutT-C) were fractioned by 12.5% SDS-polyacrylamide gel and blotted to nitrocellulose membrane. Blots were incubated with 5 µl of [^{32}P]β-NAD^+ (29.6 TBq/mmol, 185 MBq/ml) (NEN) in 10 ml of binding buffer (1 mM EDTA, 5 mM $MgCl_2$, 1% Tween 20, and 50 mM Tris-HCl, pH 7.5) for 90 min, and were washed twice with binding buffer at room temperature.

Autoradiography was at -70°C for 2 days with an intensifying screen.

Assays for cell death

Cell death was induced in HEK cells 36 h after transfection. Viability was assessed by the colorimetric 3-(4,5-dimethylthiazol-2-yl)-2,5-diphenyl tetrazolium bromide (MTT) assay and by trypan blue exclusion (Maeno et al., 2000). Changes in $[Ca^{2+}]_i$ and cell death were assessed simultaneously by observing emission of fluo-3 and PI under confocal microscope (Shimizu et al., 1998). To induce death of RIN-5F and U937 cells, 100 ng/ml TNFα with 1 ng/ml cycloheximide or 100 μM H_2O_2 was applied (6 h) in 0.5 % FBS-containing RPMI 1640.

Antisense oligonucleotide experiments

Cells were maintained with either antisense or sense oligonucleotides (5 μM) in RPMI 1640 containing 1% FBS plus antibiotics for 5 days. Alternatively, cells were maintained with oligonucleotide (20 nM) and Oligofectamine™ Reagent (Invitrogen) for 4 h in FBS- and antibiotics-free RPMI 1640, to which 10 % FBS was supplemented for next 36 h. Adherent cells were trypsinized and re-seeded on cover slips in the medium containing oligonucleotides, and used within 6-24 h for assays. The antisense and sense oligonucleotides used were 5'-ACGATGTCACCAAAGGCATC-3' and 5'-GATGCCTTTGGTGACATCGT-3', respectively, for RIN-5F, and were 5'-CTCAGGGCTGAGGGCTCCAT-3' and 5'-ATGGAGCCCTCAGCCCTGAG-3', respectively, for U937.

Western Blot Analysis

The lysates of HEK cells harvested 48 h after transfection were fractionated by 8% SDS-polyacrylamide gel, and transferred to nitrocellulose membrane as previously described (Inoue et al., 2001). Blots were incubated with anti-mLTRPC2-C1 antiserum, and stained using ECL^{TM} Western blotting analysis system (Amersham).

REFERENCES

Archer, S.L., Hampl, V., Nelson, D.P., Sidney, E., Peterson, D.A., and Weir, E.K. (1995). Dithionite increases radical formation and decreases vasoconstriction in the lung. Evidence that dithionite does not mimic alveolar hypoxia. Circ. Res. *77*, 174-181.

Barlow, R.S., El-Mowafy, A.M., and White, R.E. (2000). H_2O_2 opens BK_{Ca} channels via the PLA_2-arachidonic acid signaling cascade in coronary artery smooth muscle. Am. J. Physiol. *279*, H475-H483.

Berridge, M.J., Bootman, M.D., and Lipp, P. (1998). Calcium-a life and death signal. Nature *395*, 645-648.

Bessman, M.J., Frick, D.N., and O'Handley, S.F. (1996). The MutT proteins or "Nudix" hydrolases, a family of versatile, widely distributed, "housecleaning" enzymes. J. Biol. Chem. *271*, 25059-25062.

Bielefeldt, K., Whiteis, C.A., Sharma, R.V., Abboud, F.M., and Conklin, J.L. (1997). Reactive oxygen species and calcium homeostasis in cultured human intestinal smooth muscle cells. Am. J. Physiol. *272*, G1439-G1450.

Buisson, A., Plotkine, M., and Boulu, R.G. (1992). The neuroprotective effect of a nitric

oxide inhibitor in a rat model of focal cerebral ischaemia. Br. J. Pharmacol. *106*, 766-767.

Chiamvimonvat, N., O'Rourke, B., Kamp, T.J., Kallen, R.G., Hofmann, F., Flockerzi, V., and Marban, E. (1995). Functional consequences of sulfhydryl modification in the pore-forming subunits of cardiovascular Ca^{2+} and Na^{+} channels. Circ. Res. *76*, 325-334.

Choi, D.W. (1995). Calcium: still center-stage in hypoxic-ischemic neuronal death. Trends Neurosci. *18*, 58-60.

Chyb, S., Raghu, P., and Hardie, R.C. (1999). Polyunsaturated fatty acids activate the *Drosophila* light-sensitive channels TRP and TRPL. Nature *397*, 255-259.

Montell, C. (2001). Physiology, phylogeny,and functions of the TRP superfamily of cation channels. Science's STKE (http://www.stke.org/cgi/content/full/OC_sigtrans;2001/90/re1)

Coyle, J.T., and Puttfarcken, P. (1993). Oxidative stress, glutamate, and neurodegenerative disorders. Science *262*, 689-695.

DiChiara, T.J., and Reinhart, P.H. (1997). Redox modulation of *hslo* Ca^{2+}-activated K^{+} channels. J. Neurosci. *17*, 4942-4955.

Dunne, M.J., Findlay, I., and Petersen, O.H. (1988). Effects of pyridine nucleotides on the gating of ATP-sensitive potassium channels in insulin secreting cells. J. Membrane Biol. *102*, 205-216.

Eng, J., Lynch, R.M., and Balaban, R.S. (1989). Nicotinamide adenine dinucleotide fluorescence spectroscopy and imaging of isolated cardiac myocytes. Biophys. J. *55*, 621-630.

Fasolato, C., Innocenti, B., and Pozzan, T. (1994). Receptor-activated Ca^{2+} influx: how many mechanisms for how many channels? Trends Pharmacol. Sci. *15*, 77-83.

Freichel, M., Suh, S.H., Pfeifer, A., Schweig, U., Trost, C., Weißgerber, P., Biel, M., Philipp, S., Freise, D., Droogmans, G., Hofmann, F., Flockerzi, V., and Nilius, B. (2001). Lack of an endothelial store-operated Ca^{2+} current impairs agonist-dependent vasorelaxation in $TRP4^{-/-}$ mice. Nat. Cell Biol. *3*, 121-127.

Friedman, J.E., and Haddad, G.G. (1993). Major differences in $Ca^{2+}{}_i$ response to anoxia between neonatal and adult rat CA1 neurons: role of $Ca^{2+}{}_o$ and $Na^{+}{}_o$. J. Neurosci. *13*, 63-72.

Giroux, C., and Scatton, B. (1996). Ischemic stroke: treatment on the horizon. Eur. Neurol. *36*, 61-64.

Gotoh, Y., Cooper, J. A. (1998). Reactive oxygen species- and dimerization-induced activation of apoptosis signal-regulating kinase 1 in tumor necrosis factor-α signal transduction. J. Biol. Chem. 273, 17477-17482.

Hamill, O.P., Marty, A., Neher, E., Sakmann, B., and Sigworth, F.J. (1981). Improved patch-clamp techniques for high-resolution current recording from cells and cell-free membrane patches. Pflügers Arch. *391*, 85-100.

Hara, Y., Wakamori, M., Ishii, M, Maeno, E., Nishida, M., Yoshida, T., Yamada, H., Shimizu, S., Mori, E., Kudoh, J., Shimizu, N., Kurose, H., Okada, Y., Imoto, K., and Mori, Y. (2002). LTRPC2 Ca^{2+}-permeable channel activated by changes in redox status confers susceptibility to cell death. Mol. Cell, in press.

Harteneck, C., Plant, T.D., and Schultz, G. (2000). From worm to man: three subfamilies of TRP channels. Trends Neurosci. *23*, 159-166.

Herson, P. S., and Ashford, M. L. (1997a). Activation of a novel non-selective cation channel by alloxan and H_2O_2 in the rat insulin-secreting cell line CRI-G1. J. Physiol. *501*, 59-66.

Herson, P. S., Dulock, K. A., and Ashford, M. L. (1997b). Characterization of a nicotinamide-adenine dinucleotide-dependent cation channel in the CRI-G1 rat

insulinoma cell line. J. Physiol. *505*, 65-76.

Herson, P.S., Lee, K., Pinnock, R.D., Hughes, J., and Ashford, M.L. (1999). Hydrogen peroxide induces intracellular calcium overload by activation of a non-selective cation channel in an insulin-secreting cell line. J. Biol. Chem. *274*, 833-841.

Horn, R., and Marty, A. (1988). Muscarinic activation of ionic currents measured by a new whole-cell recording method. J. Gen. Physiol. *92*, 145-159.

Inoue, R., Okada, T., Onoue, H., Hara, Y., Shimizu, S., Naitoh, S., Ito, Y., and Mori, Y. (2001). The transient receptor potential protein homologue TRP6 is the essential component of vascular α_1-adrenoceptor-activated Ca^{2+}-permeable cation channel. Circ. Res. *88*, 325-332.

Jobling, S.A., and Gehrke, L. (1987). Enhanced translation of chimaeric messenger RNAs containing a plant viral untranslated leader sequence. Nature *325*, 622-625.

Jurman, M.E., Boland, L.M., Liu, Y., and Yellen, G. (1994). Visual identification of individual transfected cells for electrophysiology using antibody-coated beads. Biotechniques *17*, 876-881.

Kietzmann, T., Fandrey, J., and Acker, H. (2000). Oxygen radicals as messengers in

oxygen-dependent gene expression. News Physiol. Sci. *15*, 202-208.

Klonowski-Stumpe, H., Schreiber, R., Grolik, M., Schulz, H., Häussinger, D., and Niederau, C. (1997). Effect of oxidative stress on cellular functions and cytosolic free calcium of rat pancreatic acinar cells. Am. J. Physiol. *272*, G1489-G1498.

Koliwad, S.K., Elliott, S.J., and Kunze, D.L. (1996). Oxidized glutathione mediates cation channel activation in calf vascular endothelial cells during oxidant stress. J. Physiol. *495*, 37-49.

Kourie, J.I. (1998). Interaction of reactive oxygen species with ion transport mechanisms. Am. J. Physiol. *275*, C1-C24.

Kozak, M. (1986). Point mutations define a sequence flanking the AUG initiator codon that modulates translation by eukaryotic ribosomes. Cell *44*, 283-292.

Kuschel, L., Hansel, A., Schönherr, R., Weissbach, H., Brot, N., Hoshi, T., and Heinemann, S.H. (1999). Molecular cloning and functional expression of a human peptide methionine sulfoxide reductase (hMsrA). FEBS Lett. *456*, 17-21.

Li, A., Ségui, J., Heinemann, S.H., and Hoshi, T. (1998). Oxidation regulates cloned neuronal voltage-dependent Ca^{2+} channels expressed in *Xenopus* oocytes. J. Neurosci.

18, 6740-6747.

Li, E., Bestor, T.H., and Jaenisch, R. (1992). Targeted mutation of the DNA methyltransferase gene results in embryonic lethality. Cell *69*, 915-926.

Lin, S.J., Defossez, P.A., and Guarente, L. (2000). Requirement of NAD and *SIR2* for life-span extension by calorie restriction in *Saccharomyces cerevisiae*. Science *289*, 2126-2128.

Lipton, S.A., and Nicotera, P. (1998). Calcium, free radicals and excitotoxins in neuronal apoptosis. Cell Calcium *23*, 165-171.

Litt, M.R., Potter, J.J., Mezey, E., and Mitchell, M.C. (1989). Analysis of pyridine dinucleotides in cultured rat hepatocytes by high-performance liquid chromatography. Anal. Biochem. *179*, 34-36.

Maeno, E., Ishizaki, Y., Kanaseki, T., Hazama, A., and Okada, Y. (2000). Normotonic cell shrinkage because of disordered volume regulation is an early prerequisite to apoptosis. Proc. Natl. Acad. Sci. USA *97*, 9487-9492.

Mattson, M.P. (1996). Calcium and free radicals: mediators of neurotrophic factor and excitatory transmitter-regulated developmental plasticity and cell death. Perspect. Dev.

Neurobiol. *3*, 79-91.

Mendez, F., and Penner, R. (1998). Near-visible ultraviolet light induces a novel ubiquitous calcium-permeable cation current in mammalian cell lines. J. Physiol. *507*, 365-377.

Nadler, M.J., Hermosura, M.C., Inabe, K., Perraud, A.L., Zhu, Q., Stokes, A.J., Kurosaki, T., Kinet, J.P., Penner, R., Scharenberg, A.M., and Fleig, A. (2001). LTRPC7 is a Mg·ATP-regulated divalent cation channel required for cell viability. Nature *411*, 590-595.

Nagamine, K., Kudoh, J., Minoshima, S., Kawasaki, K., Asakawa, S., Ito, F., and Shimizu, N. (1998). Molecular cloning of a novel putative Ca^{2+} channel protein (TRPC7) highly expressed in brain. Genomics *54*, 124-131.

Nishida, M., Nagao, T., and Kurose, H. (1999). Activation of Rac1 increases c-jun NH_2-terminal kinase activity and DNA fragmentation in a calcium-dependent manner in rat myoblast cell line H9c2. Biochem. Biophys. Res. Commun. *262*, 350-354.

Okada, T., Shimizu, S., Wakamori, M., Maeda, A., Kurosaki, T., Takada, N., Imoto, K., and Mori, Y. (1998). Molecular cloning and functional characterization of a novel receptor-activated TRP Ca^{2+} channel from mouse brain. J. Biol. Chem. *273*,

10279-10287.

Okamoto, H. (1985). Molecular basis of experimental diabetes: degeneration oncogenesis and regeneration of pancreatic B-cells of islets of Langerhans. BioEssays *2*, 15-21.

Patel, A.J., Honoré, E., Maingret, F., Lesage, F., Fink, M., Duprat, F., and Lazdunski, M. (1998). A mammalian two pore domain mechano-gated S-like K^+ channel. EMBO J. *17*, 4283-4290.

Perraud, A-L., Fleig, A., Dunn, C.A., Bagley, L.A., Launay, P., Schmitz, C., Stokes, A.J., Zhu, Q., Bessman, M.J., Penner, R., Kinet, J-P., and Scharenberg, A.M. (2001). ADP-ribose gating of the calcium-permeable LTRPC2 channel revealed by Nudix motif homology. Nature *411*, 595-599.

Runnels, L.W., Yue, L., Clapham, D.E. (2001). TRP-PLIK, a bifunctional protein with kinase and ion channel activities. Science *291*, 1043-1047.

Ruppersberg, J.P., Stocker, M., Pongs, O., Heinemann, S.H., Frank, R., and Koenen, M. (1991). Regulation of fast inactivation of cloned mammalian $I_K(A)$ channels by cysteine oxidation. Nature *352*, 711-714.

Sano, Y., Imamura, K., Miyake, A., Mochizuki, S., Yokoi, H., Matsushime, H., and

Furuichi, K. (2001). Immunocyte Ca^{2+} influx system mediated by LTRPC2. Science *293*, 1327-1330.

Shimizu, S., Nomoto, M., Naito, S., Yamamoto, T., and Momose, K. (1998). Stimulation of nitric oxide synthase during oxidative endothelial cell injury. Biochem. Pharmacol. *55*, 77-83.

Trepakova, E.S., Cohen, R.A., and Bolotina, V.M. (1999). Nitric oxide inhibits capacitative cation influx in human platelets by promoting sarcoplasmic/endoplasmic reticulum Ca^{2+}-ATPase-dependent refilling of Ca^{2+} stores. Circ. Res. *84*, 201-209.

Tretter, L., and Adam-Vizi, V. (2000). Inhibition of Krebs cycle enzymes by hydrogen peroxide: A key role of α-ketoglutarate dehydrogenase in limiting NADH production under oxidative stress. J. Neurosci. *20*, 8972-8979.

Ueno, M., Masutani, H., Arai, R.J., Yamauchi, A., Hirota, K., Sakai, T., Inamoto, T., Yamaoka, Y., Yodoi, J., and Nikado, T. (1999). Thioredoxin-dependent redox regulation of p53-mediated p21 activation. J. Biol. Chem. *274*, 35809-35815.

Vercammen, D., Beyaert, R., Denecker, G., Goossens, V., Van Loo, G., De-clercq, W.,Grooten, J., Fiers, W., and Vandenabeele, P. (1998a). Inhibition of caspases increases the sensitivity of L929 cells to necrosis mediated by tumor necrosis factor. J.

Exp. Med. *187*, 1477–1485.

Vercammen, D., Brouckaert, G., Denecker, G., Van de Craen, M., Declercq, W., Fiers, W., and Vandenabeele, P. (1998b). Dual signaling of the Fas receptor: initiation of both apoptotic and necrotic cell death pathways. J. Exp. Med. *188*, 919–930.

Wakamori, M., Hidaka, H., and Akaike, N. (1993). Hyperpolarizing muscarinic responses of freshly dissociated rat hippocampal CA1 neurones. J. Physiol. *463*, 585-604.

Wink, D.A., Hanbauer, I., Krishna, M.C., DeGraff, W., Gamson, J., and Mitchell, J.B. (1993). Nitric oxide protects against cellular damage and cytotoxicity from reactive oxygen species. Proc. Natl. Acad. Sci. USA *90*, 9813-9817.

Xu, L., Eu, J.P., Meissner, G., and Stamler, J.S. (1998). Activation of the cardiac calcium release channel (ryanodine receptor) by poly-S-nitrosylation. Science *279*, 234-237.

Ziegler, M. (2000). New functions of a long-known molecule. Emerging roles of NAD in cellular signaling. Eur. J. Biochem. *267*, 1550-1564.

Figure 1

A

```
hLTRPC2 MEPSALRKAGSEQEEGFEGLPRRVTDLGMVSNLRRSNSSLFKSWRLQCPFGNNDKQESLSSWIPENIKKKECVYFVESSKLSDAGKVVCQCGYTHEQHLEEATKPHTFQGTQWDPKKHVQ   1 - 120
mLTRPC2 MESLDRRRTGSEQEEGFGVQSRRATDLGMVPNLRRSNSSLCKSRRFLCSFSS-EKQENLSSWIPENIKKKECVYFVESSKLSDAGKVVCACGYTHEQHLEVAIKPHTFQGKEWDPKKHVQ   1 - 119

        EMPTDAFGDIVFTGLSQKVKKYVRVSQDTPSSVIYHLMTQHWGLDVPNLLISVTGGAKNFNMKPRLKSIFRRGLVKVAQTTGAWIITGGSHTGVMKQVGEAVRDFSLSSSYKEGELITIG   121 - 240
        EMPTDAFGDIVFTDLSQKVGKYVRVSQDTPSSVIYQLMTQHWGLDVPNLLISVTGGAKNFNMKLRLKSIFRRGLVKVAQTTGAWIITGGSHTGVMKQVGEAVRDFSLSSSCKEGEVITIG   120 - 239

        VATWGTVHRREGLIHPTGSFPAEYILDEDGQGNLTCLDSNHSHFILVDDGTHGQYGVEIPLRTRLEKFISEQTKERGGVAIKIPIVCVVLEGGPGTLHTIDNATTNGTPCVVVEGSGRVA   241 - 360
        VATWGTIHNREGLIHPMGGFPAEYMLDEEGQGNLTCLDSNHSHFILVDDGTHGQYGVEIPLRTKLEKFISEQTKERGGVAIKIPIVCVVLEGGPGTLHTIYNAINNGTPCVIVEGSGRVA   240 - 359

        DVIAQVANLPVSDITISLIQQKLSVFFQEMFETFTESRIVEWTKKIQDIVRRRQLLTVFREGKDGQQDVDVAILQALLKASRSQDHFGHENWDHQLKLAVAWNRVDIARSEIFMDEWQWK   361 - 480
        DVIAQVATLPVSEITISLIQQKLSIFFQEMFETFTENQIVEWTKKIQDIVRRRQLLTIFREGKDGQQDVDVAILQALLKASRSQDHFGHENWDHQLKLAVAWNRVDIARSEIFTDEWQWK   360 - 479

        PSDLHPTMTAALISNKPEFVKLFLENGVQLKEFVTWDTLLYLYENLDPSCLFHSKLQKVLVEDPERPACAPAAPRLQMHHVAQVLRELLGDFTQPLYPRPRHNDRLRLLLPVPHVKLNVQ   481 - 600
        PADLHPMTTAALISNKPEFVRLFLENGVRLKEFVTWDTLLCLYENLEPSCLFHSKLQKVLAEE-QRLAYASATPRLHMHHVAQVLRELLGDSTQLLYPRPRYTDRPRLSMTVPHIKLNVQ   480 - 598

        GVSLRSLYKRSSGHVTFTMDPIRDLLIWAIVQNRRELAGIIWAQSQDCIAAALACSKILKELSKEEEDTDSSEEMLALAEEYEHRAIGVFTECYRKDEERAQKLLTRVSEAWGKTTCLQL   601 - 720
        GVSLRSLYKRSTGHVTFTIDPVRDLLIWAVIQNHRELAGIIWAQSQDCTAAALACSKILKELSKEEEDTDSSEEMLALADEFEHRAIGVFTECYRKDEERAQKLLVRVSEAWGKTTCLQL   599 - 718

        ALEAKDMKFVSHGGIQAFLTKVWWGQLSVDNGLWRVTLCMLAFPLLLTGLISFREKRLQDVGTPAARARAFFTAPVVVFHLNILSYFAFLCLFAYVLMVDFQPVPSWCECAIYLWLFSLV   721 - 840
        ALEAKDMKFVSHGGIQAFLTKVWWGQLCVDNGLWRIILCMLAFPLLFTGFISFREKRLQALCRPAR-VRAFFNAPVVIFHMNILSYFAFLCLFAYVLMVDFQPSPSWCEYLIYLWLFSLV   719 - 837
                                           H1                                      H2                  H3
        CEEMRQLFYDPDECGLMKKAALYFSDFWNKLDVGAILLFVAGLTCRLIPATLYPGRVILSLDFILFCLRLMHIFTISKTLGPKIIIVKRMMKDVFFFLFLLAVWVVSFGVAKQAILIHNE   841 - 960
        CEETRQLFYDPDGCGLMKMASLYFSDFWNKLDVGAILLFIVGLTCRLIPATLYPGRIILSLDFIMFCLRLMHIFTISKTLGPKIIIVKRMMKDVFFFLFLLAVWVVSFGVAKQAILIHNE   838 - 957
                                   H4                H5                        H6
        RRVDWLFRGAVYHSYLTIFGQIPGYIDGVNFNPEHCSPNGTDPYKPKCPESDATQQRPAFPEWLTVLLLCLYLLFTNILLLNLLIAMFNYTFQQVQEHTDQIWKFQRHDLIEEYHGRPAA   961 - 1080
        SRVDWIFRGVVYHSYLTIFGQIPTYIDGVNFSMDQCSPNGTDPYKPKCPESDWTGQAPAFPEWLTVTLLCLYLLFANILLLNLLIAMFNYTFQEVQEHTDQIWKFQRHDLIEEYHGRPPA   958 - 1077
             H7                                        H8
        PPPFILLSHLQLFIKRVVLKTPAKRHKQLKNKLEKNEEAALLSWEIYLKENYLQNRQFQQKQRPEQKIEDISNKVDAMVDLLDLDPLKRSGSMEQRLASLEEQVAQTARALHWIVRTLRA   1081 - 1200
        PPPLILLSHLQLLIKRIVLKIPAKRHKQLKNKLEKNEETALLSWELYLKENYLQNQQYQQKQRPEQKIQDISEKVDTMVDLLDMDQVKRSGSTEQRLASLEEQVTQVTRALHWIVTTLKD   1078 - 1197

        SGFSSEADVPTLASQKAAEEPDAEPGGRKKTEEPGDSYHVNARHLLYPNCPVTRFPVPNEKVPWETEFLIYDPPFYTAERKDAAAMDPMGDTLEPLSTIQYNVVDGLRDRRSFHGPYTVQ   1201 - 1320
        SGFGSGAGALTLAPQRAFDEPDAELSIRRKVEEPGDGYHVSARHLLYPNARIMRFPVPNEKVPWAAEFLIYDPPFYTAEK-DVALTDPVGDTAEPLSKISYNVVDGPTDRRSFHGVYVVE   1198 - 1316

        AGLPLNPMGRTGLRGRGSLSCFGPNHTLYPMVTRWRRNEDGAICRKSIKKMLEVLVVKLPLSEHWALPGGSREPGEMLPRKLKRILRQEHWPSFENLLKCGMEVYKGYMDDPRNTDNAWI   1321 - 1440
        YGFPLNPMGRTGLRGRGSLSWFGPNHTLQPVVTRWKRNQGGAICRKSVRKMLEVLVMKLPRSEHWALPGGSREPGEMLPRKLKRVLRQEFWVAFETLLMQGTEVYKGYVDDPRNTDNAWI   1317 - 1436

        ETVAVSVHFQDQNDVELNRLNSNLHACDSG-------ASIRWQVVDRRIPLYANHKTLLQKAAAEFGAHY                                                 1441 - 1503
        ETVAVSIHFQDQNDMELKRLEENLHTHDPKELTRDLKLSTEWQVVDRRIPLYANHKTLLQKVASLFGAHF                                                 1437 - 1506
```

B

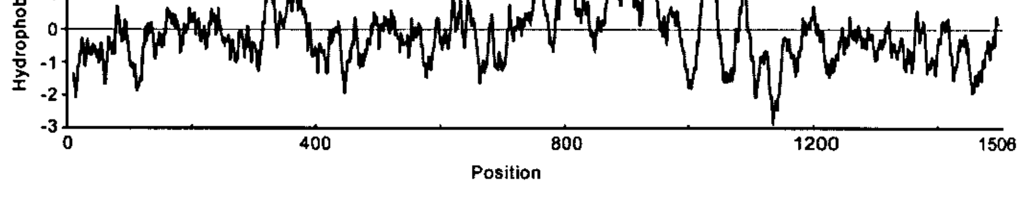

Figure 1. Primary structure of mouse LTRPC2.

(A) The amino acid sequence (in *single letter code*) of human and mouse LTRPC2 aligned using the Clustal W program. Pairs of identical amino acids are marked with asterisks. Arachidonic acid responsive sequence (ARS) and MutT motif are boxed with a solid line. The hydrophobic regions H1-H8 are shown (See Figure 7).

(B) The Kyte-Doolittle hydrophobicity profile was generated with the window size of 15 amino acids.

Figure 2

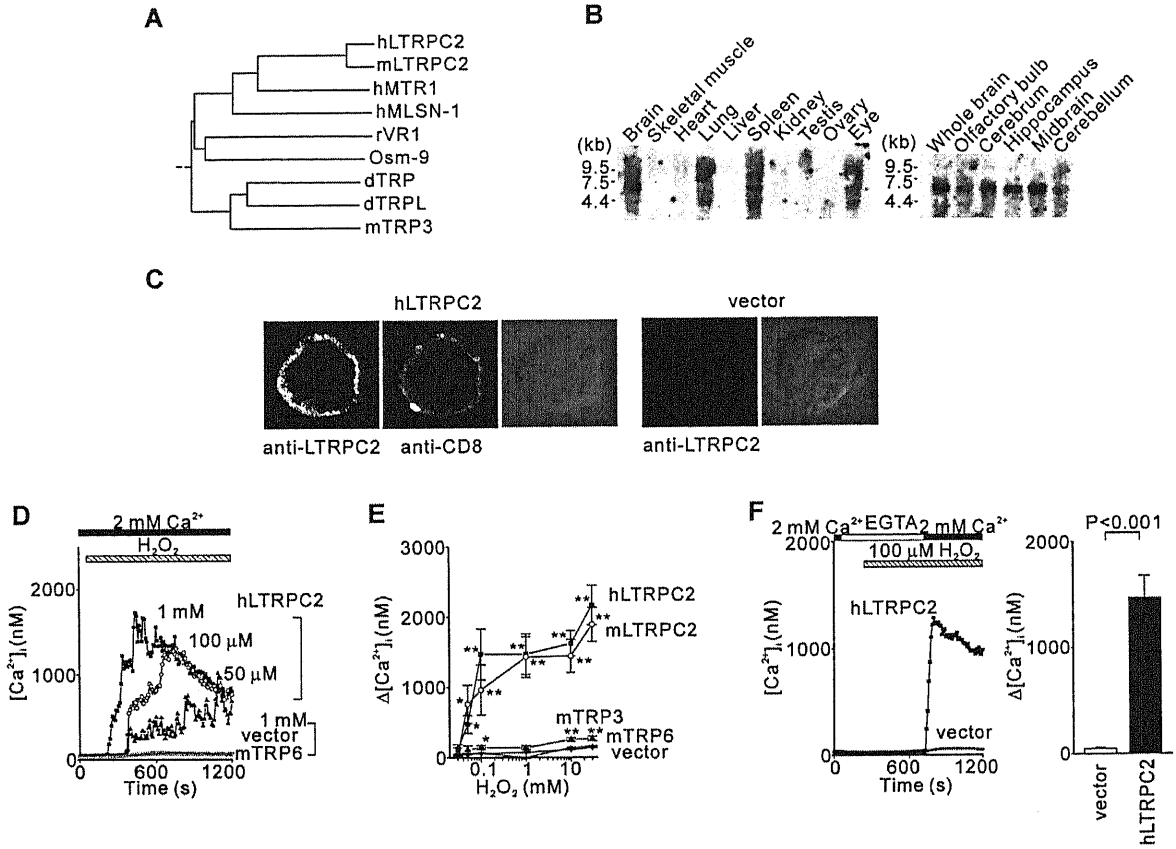
A
hLTRPC2
mLTRPC2
hMTR1
hMLSN-1
rVR1
Osm-9
dTRP
dTRPL
mTRP3
B
(kb)
Brain
Skeletal muscle
Heart
Lung
Liver
Spleen
Kidney
Testis
Ovary
Eye
9.5
7.5
4.4
(kb)
Whole brain
Olfactory bulb
Cerebrum
Hippocampus
Midbrain
Cerebellum
9.5
7.5
4.4
C
hLTRPC2
vector
anti-LTRPC2
anti-CD8
anti-LTRPC2
D
2 mM Ca2+
H2O2
2000
1000
0
[Ca2+]i (nM)
hLTRPC2
1 mM
100 μM
50 μM
1 mM
vector
mTRP6
0
600
1200
Time (s)
E
3000
2000
1000
0
Δ[Ca2+]i (nM)
hLTRPC2
mLTRPC2
mTRP3
mTRP6
vector
0.1
1
10
H2O2 (mM)
F
2 mM Ca2+
EGTA
2 mM Ca2+
100 μM H2O2
2000
1000
0
[Ca2+]i (nM)
hLTRPC2
vector
0
600
1200
Time (s)
P<0.001
2000
1000
0
Δ[Ca2+]i (nM)
vector
hLTRPC2

Figure 2. Activation of LTRPC2-mediated Ca^{2+} entry by H_2O_2.

(A) Phylogenetic tree for the TRP superfamily: hLTRPC2 (GenBank accession No. AB001535), mLTRPC2, human melastatin 1 and TRPC7 related protein 1 (hMTR1) (AF177473), human melastatin 1 (hMLSN-1) (AF071787), rat VR1 (AF029310), *Drosophila* Osm-9 (AF031408), *Drosophila* TRP (M21306), *Drosophila* TRPL (M88185), and mouse TRP3 (mTRP3) (AF190645). The CLUSTAL W program was used.

(B) Northern blot analysis of LTRPC2 RNA distribution in mouse tissues and in the brain.

(C) Confocal immunoimmages of LTRPC2 protein localization using an antiserum to the C-terminus of mLTRPC2 and FITC-labeled anti-rabbit goat antiserum in hLTRPC2- and vector-transfected HEK cells. Co-expressed CD8 was detected using the monoclonal antibody against human CD8 (B9.2; Immunotech) and rhodamine-labeled anti-mouse $F(ab')_2$ fragment. The corresponding differential interference contrast (DIC) images are also shown.

(D and E) H_2O_2-induced $[Ca^{2+}]_i$ changes detected in single hLTRPC2-, mLTRPC2-, mTRP3-, mouse TRP6 (mTRP6)-, and vector-transfected HEK cells in the presence of 2 mM extracellular Ca^{2+}. Mean responses (D) and dose-response relationships for maximum $[Ca^{2+}]_i$ rises ($\Delta[Ca^{2+}]_i$) induced by H_2O_2 (E). Data points are the means ± S.E. $\Delta[Ca^{2+}]_i$. * and ** indicate $P<0.05$ and $P<0.001$, respectively, compared with vector-transfected cells.

(F) LTRPC2 mediates Ca^{2+}-entry in response to H_2O_2. Left, after 8 min exposure to 100 μM H_2O_2 in Ca^{2+}-free, 0.5 mM EGTA-containing solution, LTRPC2-expressing cells were exposed to the solution containing 2 mM Ca^{2+} and 100 μM H_2O_2. Right,

maximum H_2O_2-induced $[Ca^{2+}]_i$ rises after re-addition of external Ca^{2+}.

Figure 3

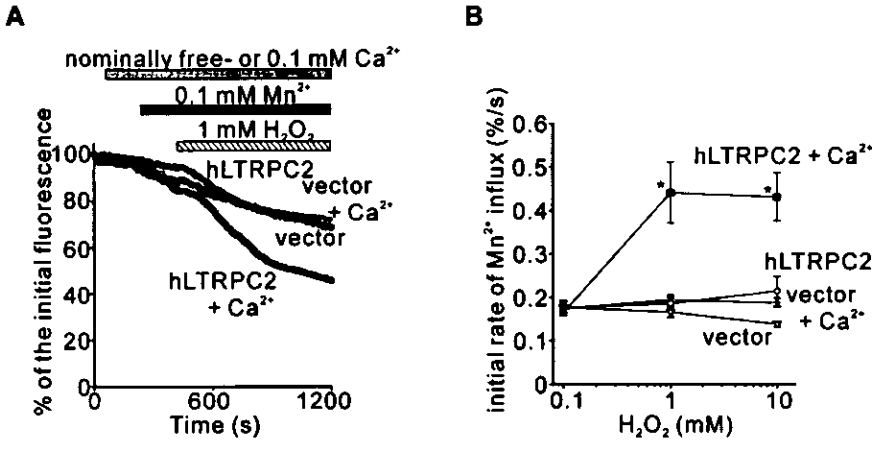
A
nominally free- or 0.1 mM Ca2+
0.1 mM Mn2+
1 mM H2O2
hLTRPC2
vector
+ Ca2+
vector
hLTRPC2
+ Ca2+
% of the initial fluorescence
100
80
60
40
20
0
0
600
1200
Time (s)
B
initial rate of Mn2+ influx (%/s)
0.6
0.5
0.4
0.3
0.2
0.1
0
hLTRPC2 + Ca2+
hLTRPC2
vector
+ Ca2+
vector
0.1
1
10
H2O2 (mM)

Figure 3. Dependency of LTRPC2-mediated Mn^{2+} influx on extracellular Ca^{2+}.

(A) H_2O_2 (1 mM)-induced Mn^{2+} influx was observed in the presence and absence of 0.1 mM Ca^{2+}, in hLTRPC2- and vector-transfected cells.

(B) Rates for initial phase of H_2O_2-induced Mn^{2+} quenching.

Figure 4

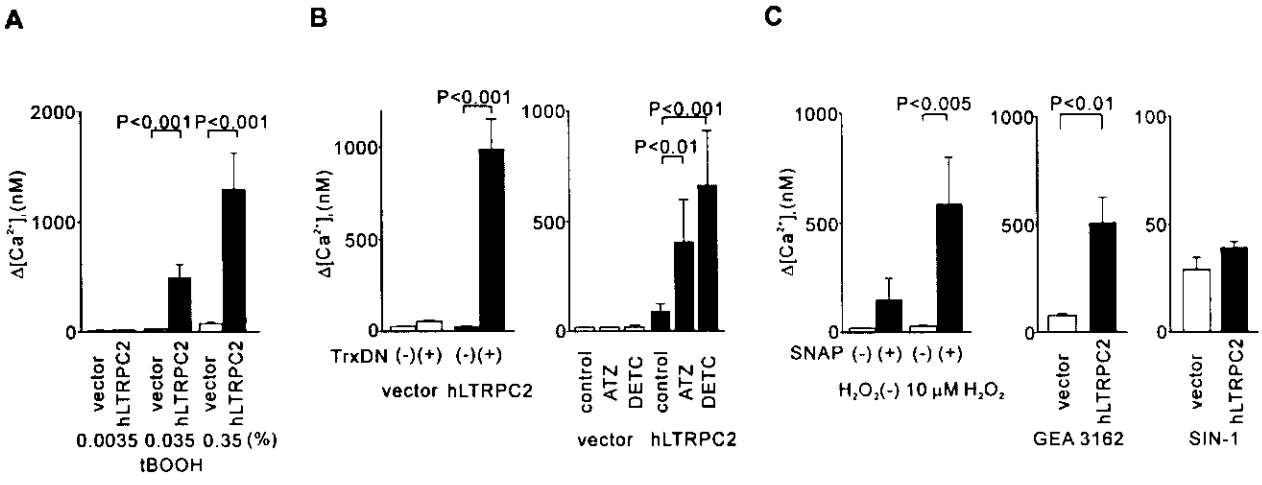
A
B
C
Δ[Ca2+]i (nM)
2000
1000
0
P<0.001
P<0.001
P<0.001
vector
hLTRPC2
vector
hLTRPC2
vector
hLTRPC2
0.0035 0.035 0.35 (%)
tBOOH
1000
500
0
P<0.001
TrxDN (-)(+) (-)(+)
vector hLTRPC2
1000
500
0
P<0.001
P<0.01
control
ATZ
DETC
control
ATZ
DETC
vector hLTRPC2
1000
500
0
P<0.005
SNAP (-) (+) (-) (+)
H2O2(-) 10 μM H2O2
1000
500
0
P<0.01
vector
hLTRPC2
GEA 3162
100
50
0
vector
hLTRPC2
SIN-1

Figure 4. LTRPC2 is activated by ROS- or RNS-generating agents.

(A) $[Ca^{2+}]_i$ rises induced by tBOOH in LTRPC2-expressing cells in the presence of 2 mM Ca^{2+}.

(B) Perturbation of endogenous antioxidants elicits LTRPC2-mediated $[Ca^{2+}]_i$ elevation in response to H_2O_2 of subthreshold concentration (10 μM). The dominant negative mutant of thioredoxin was coexpressed (Trx DN) (+), or ATZ (1 mM) and DETC (1 mM) were loaded using non-ionic, sulfactant polyol Pluronic® F-127 (Molecular Probes) from 2.5 h prior to measurements.

(C) Maximum $[Ca^{2+}]_i$ rises in LTRPC2-expressing cells treated with SNAP (300 μM) (left), GEA 3162 (100 μM) (middle), or SIN-1 (1 mM) (right).

Figure 5

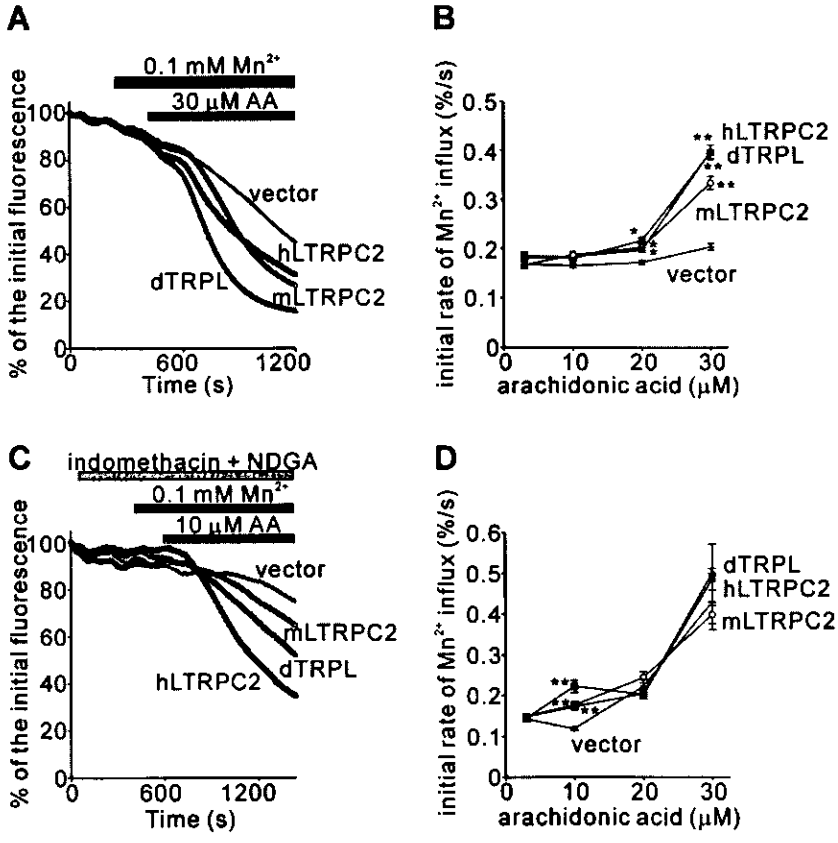
A
0.1 mM Mn2+
30 μM AA
vector
hLTRPC2
dTRPL
mLTRPC2
% of the initial fluorescence
Time (s)
B
initial rate of Mn2+ influx (%/s)
hLTRPC2
dTRPL
mLTRPC2
vector
arachidonic acid (μM)
C
indomethacin + NDGA
0.1 mM Mn2+
10 μM AA
vector
mLTRPC2
dTRPL
hLTRPC2
% of the initial fluorescence
Time (s)
D
initial rate of Mn2+ influx (%/s)
dTRPL
hLTRPC2
mLTRPC2
vector
arachidonic acid (μM)

Figure 5. AA-induced Mn^{2+} influx in hLTRPC2-, mLTRPC2-, *Drosophila* TRPL-, or vector-transfected cells.

(A) Quenching of fura-2 fluorescence by Mn^{2+} entry. Thirty μM AA was applied after addition of 0.1 mM Mn^{2+} to nominally Ca^{2+}-free HBS. (B) Rates for initial phase of AA-induced reduction of fluorescence. Data points are the means ± S.E. percentage reduction of fluorescence. * and ** indicate $P<0.05$ and $P<0.001$, respectively. (C) AA-induced Mn^{2+} quenching in the presence of NDGA (20 μM) and indomethacin (20 μM) applied 10 min before AA application (10 μM). (D) Rates for initial phase of AA-induced Mn^{2+} quenching in the presence of the blockers.

Figure 6

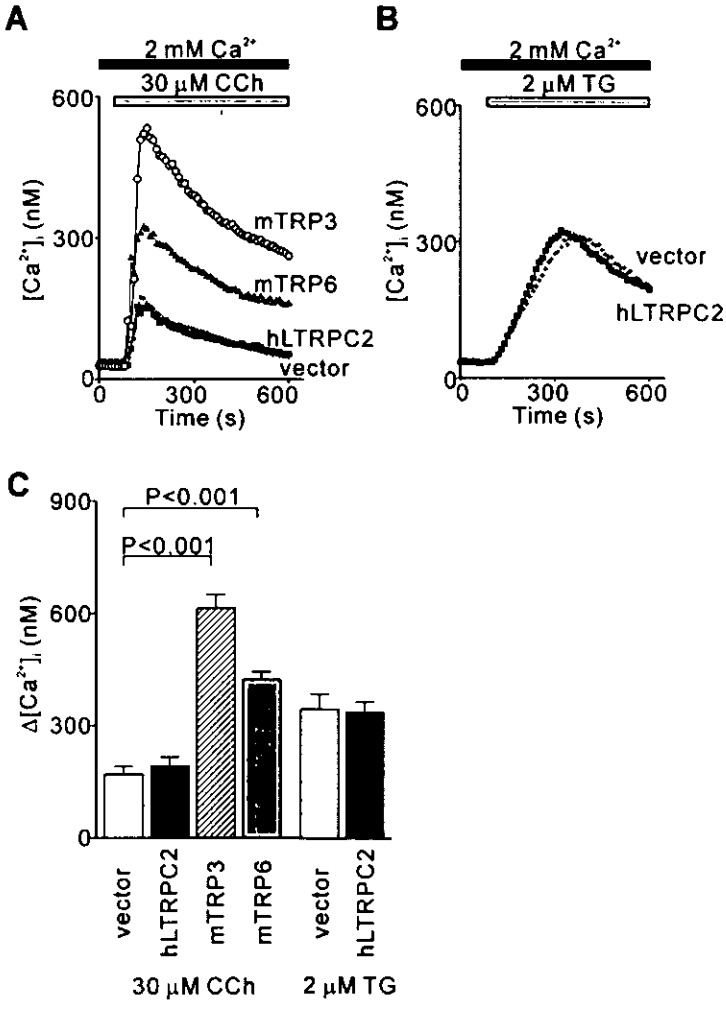
A
2 mM Ca2+
30 μM CCh
600
300
0
[Ca2+]i (nM)
mTRP3
mTRP6
hLTRPC2
vector
0
300
600
Time (s)
B
2 mM Ca2+
2 μM TG
600
300
0
[Ca2+]i (nM)
vector
hLTRPC2
0
300
600
Time (s)
C
900
600
300
0
Δ[Ca2+]i (nM)
P<0.001
P<0.001
vector
hLTRPC2
mTRP3
mTRP6
vector
hLTRPC2
30 μM CCh
2 μM TG

Figure 6. $[Ca^{2+}]_i$ transients induced by CCh (30 μM) and TG (2 μM) in hLTRPC2-transfected HEK cells.

(A) $[Ca^{2+}]_i$ responses induced by stimulation of muscarinic receptors in hLTRPC2-, mTRP3-, mTRP6-, and vector-transfected HEK cells. The duration of exposure to Ca^{2+}-containing HBS, CCh indicated by the bars above traces.

(B) $[Ca^{2+}]_i$ responses induced by depletion of internal Ca^{2+} stores by TG (2 μM) in hLTRPC2- and vector-transfected HEK cells. The duration of exposure to Ca^{2+}-containing HBS, CCh indicated by the bars above traces.

(C) Maximum $[Ca^{2+}]_i$ rises induced by CCh and TG (means ± S.E. $\Delta[Ca^{2+}]_i$).

Figure 7

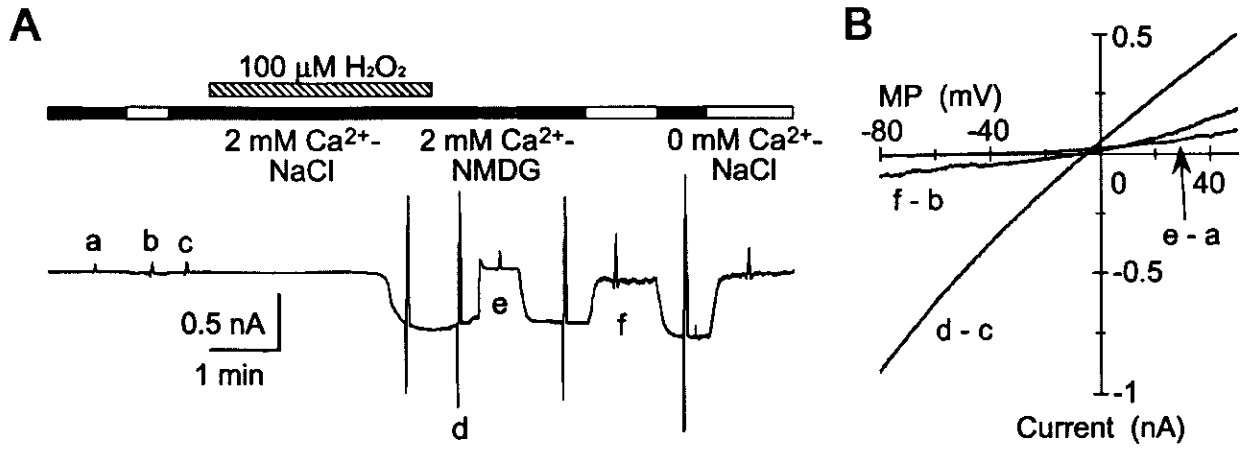
A
100 µM H2O2
2 mM Ca2+-
NaCl
2 mM Ca2+-
NMDG
0 mM Ca2+-
NaCl
a
b
c
d
e
f
0.5 nA
1 min
B
MP (mV)
-80
-40
0
40
0.5
-0.5
-1
f - b
e - a
d - c
Current (nA)

Figure 7. Whole-cell LTRPC2 currents induced by H_2O_2.

(A) Typical whole-cell currents in nystatin-perforated configuration at a V_h of -50 mV. Two-seconds triangular voltage ramps from -100 mV to 60 mV were applied. Horizontal bars above each trace indicate the duration of application of 2 mM Ca^{2+}-NaCl solution (*filled bars*), 0 mM Ca^{2+}-NaCl solution (*open bars*), 2 mM Ca^{2+}-NMDG solution (*shaded bars*), and 100 μM H_2O_2 (*hatched bar*). (B) I-V relationships of the H_2O_2-induced LTRPC2 current, obtained by subtracting currents before activation of channels from those after activation (indicated by small letters in (A)).

Figure 8

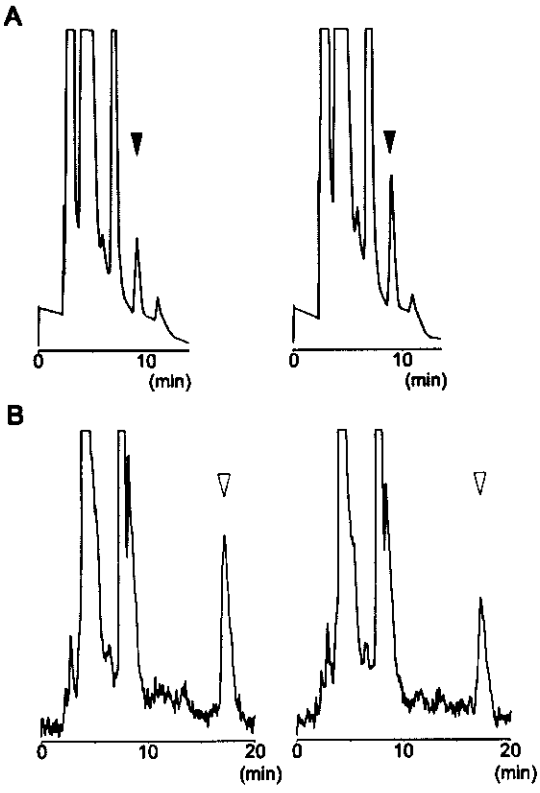
A
0
10
(min)
0
10
(min)
B
0
10
20
(min)
0
10
20
(min)

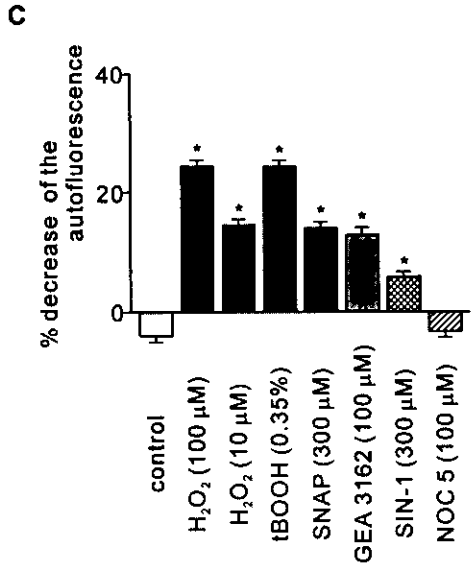
C
% decrease of the autofluorescence
40
20
0
control
H2O2 (100 µM)
H2O2 (10 µM)
tBOOH (0.35%)
SNAP (300 µM)
GEA 3162 (100 µM)
SIN-1 (300 µM)
NOC 5 (100 µM)

Figure 8. HPLC and fluorescent analysis of endogenous NAD^+ or NADH in H_2O_2-treated HEK cells.

(A) Chromatogram of NAD^+ for control (left panel) and 30 μM H_2O_2-treated (5 min) HEK cells (right panel). *Filled arrowheads* indicate the peak of NAD^+.

(B) Chromatogram of NADH for control (left panel) and 30 μM H_2O_2-treated (5 min) HEK cells (right panel). *Open arrowheads* indicate the peak of NADH.

(C) Percentage reduction of NAD(P)H antofluorescence intensity during exposure to ROS- or RNS-generating agents in HEK cells. The changes of NAD(P)H autofluorescence in HEK cells were observed using excitation at 360 nm and emission at 460 nm without loading fura-2/AM. The reduction was calculated 400 sec after the addition of ROS- or RNS-generating agents. Elevation of $[Ca^{2+}]_i$ in LTRPC2-expressing HEK cells was clearly observed at 6 min after addition of 100 μM H_2O_2 (Figure 2D). Data represents the mean ± S.E.. * indicate $P<0.001$ compared with control HEK cells.

Figure 9

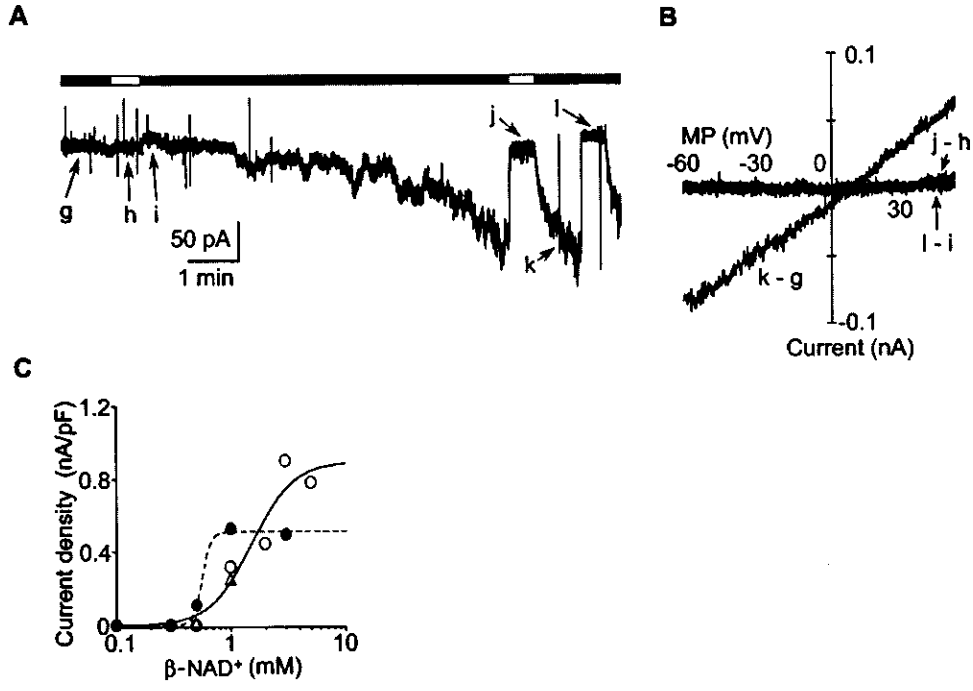
A
g
h
i
j
l
k
50 pA
1 min
B
0.1
MP (mV)
-60
-30
0
30
j - h
l - i
k - g
-0.1
Current (nA)
C
Current density (nA/pF)
1.2
0.8
0.4
0
0.1
1
10
β-NAD+ (mM)

Figure 9 Activation of LTRPC2 channel currents by β-NAD^+

(A) Activation of the LTRPC2 current recorded using the conventional whole-cell mode of patch clamp. One mM β-NAD^+ was added to the pipette solution. The current observed within 20 s after the formation of whole-cell configuration was omitted. 0.2-s triangular voltage ramps were applied from a V_h of -50 mV.

(B) I-V relationships of the β-NAD^+-induced LTRPC2 current.

(C) Dose-response curve relating intrapipette β-NAD^+ concentration to LTRPC2 current density (*open circles*) (apparent K_D, 1.8 mM; Hill coefficient, 2.2), and that obtained when AA was applied (*closed circles*) (apparent K_D, 0.56 mM; Hill coefficient, 11.5). *Open triangles* are current densities obtained by dialyzing cells with β-NAD^+ plus NADH (50 μM), $NADP^+$ (70 μM), NADPH (50 μM), ADP (800 μM), and ATP (2 mM) from the patch pipette.

Figure 10

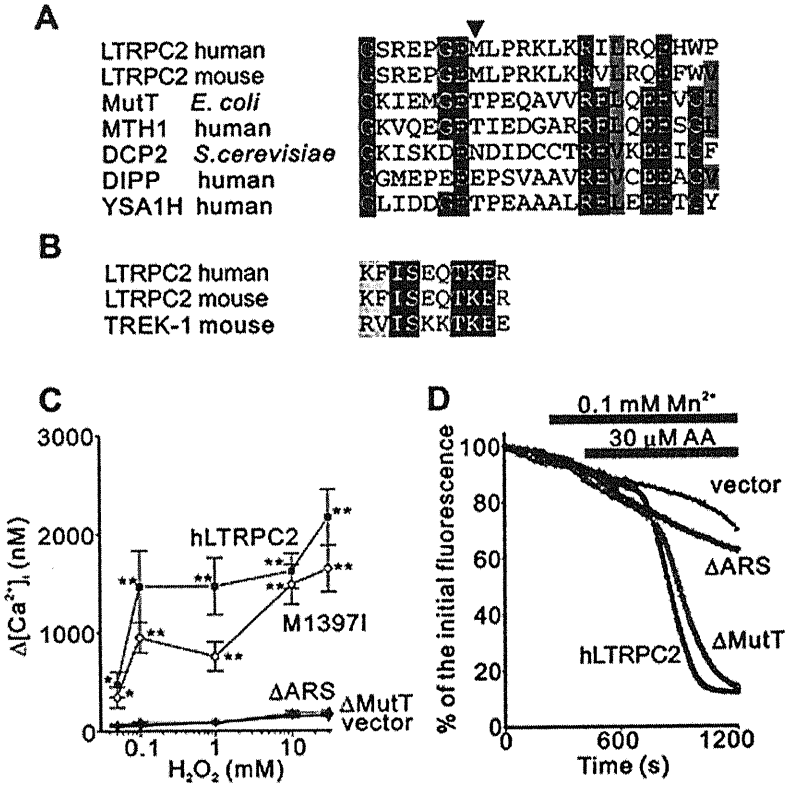
A
LTRPC2 human
LTRPC2 mouse
MutT E. coli
MTH1 human
DCP2 S.cerevisiae
DIPP human
YSA1H human
B
LTRPC2 human
LTRPC2 mouse
TREK-1 mouse
C
hLTRPC2
M1397I
ΔARS
ΔMutT
vector
Δ[Ca2+]i (nM)
H2O2 (mM)
D
0.1 mM Mn2+
30 μM AA
vector
ΔARS
ΔMutT
hLTRPC2
% of the initial fluorescence
Time (s)

Figure 10 MutT motif and AA-responsive sequence (ARS) essential for activation of the LTRPC2 channel.

(A) Alignment of the MutT sequences in hLTRPC2 (residues 1390-1412) and mLTRPC2 (1386-1408) with those in *E.coli* MutT (P08337), human MTH1 (AB025233), *S.cerevisiae* DCP2 (YSCPSU1A), human diphosphoinositol polyphosphate phosphohydrolase (DIPP) (AF062529), and human YSA1H (AF155832). The residues well conserved among the aligned sequences and the bulky aliphatic amino acids are indicated by black and gray boxes, respectively. The arrowhead indicates M1397.

(B) Alignment of the ARS in hLTRPC2 (307-316), mLTRPC2 (306-315), and TREK-1 (297-306) (Patel et al., 1998). The conserved residues and chemically similar residues are indicated by black and gray boxes, respectively.

(C) H_2O_2 concentration dependence of maximum $[Ca^{2+}]_i$ rises in hLTRPC2-, M1397I-, ΔARS-, ΔMutT-, and vector-transfected cells. The MutT (1390-1409) or ARS (307-316) was deleted in ΔMutT or ΔARS, respectively. Data points are the means ± S.E. $\Delta[Ca^{2+}]_i$. * and ** indicate $P<0.05$ and $P<0.001$, respectively.

(D) AA (30 μM)-induced Mn^{2+} influx in hLTRPC2-, ΔMutT-, ΔARS-, and vector-transfected cells.

Figure 11

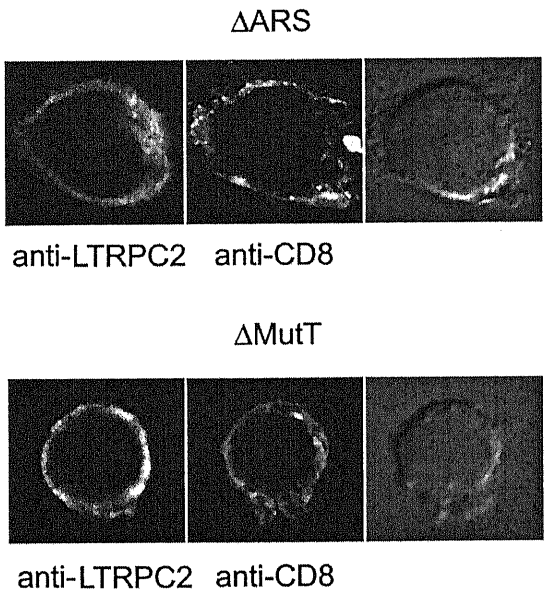

Figure 11 Membrane localization of the LTRPC2 mutant lacking ARS (ΔARS) or MutT (ΔMutT) in transiently transfected in HEK cells.

The mutants and CD8 protein were detected using anti-mLTRPC2-C1 antiserum or anti-human CD8 antibody. The corresponding DIC images are also shown.

Figure 12

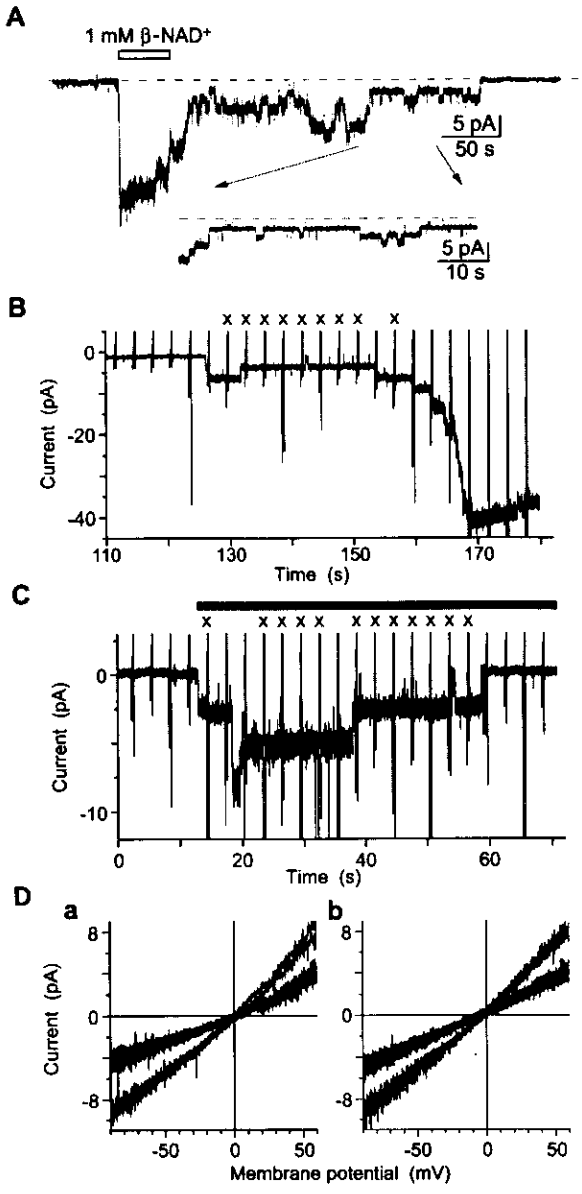
A
1 mM β-NAD+
5 pA
50 s
5 pA
10 s
B
Current (pA)
0
-20
-40
110
130
150
170
Time (s)
C
Current (pA)
0
-10
0
20
40
60
Time (s)
D
a
b
Current (pA)
8
0
-8
-50
0
50
Membrane potential (mV)

Figure 12 Single-channel properties of the LTRPC2 channel.

(A) Activation of single LTRPC2 channel currents by β-NAD^+ in cell-free, excised inside-out membrane patches at a V_h of -50 mV. The segment indicated by the arrows is expanded on a faster time scale (*inset*).

(B) Single-channel currents recorded at a V_h of -50 mV in cell-attached patch configuration from hLTRPC2-expressing cells continuously treated with 100 μM H_2O_2 from outside of the patch. The trace without unitary activity for initial 110 s H_2O_2 application was omitted. 330-ms triangular voltage ramps from –90 mV to 60 mV were applied every 3 s.

(C) Single-channel currents activated at a V_h of –50 mV by 3 mM β-NAD^+ applied to the inner surface of the patch membrane excised from LTRPC2-expressing cells in inside-out patch configuration. The same voltage ramps as in (B).

(D) Subtracted I-V relationships of the single LTRPC2 channel. (a) and (b) from (B) and (C), respectively. The average of currents at the level 0 was subtracted from the currents with marks (x) at the level 1 or 2.

Figure 13

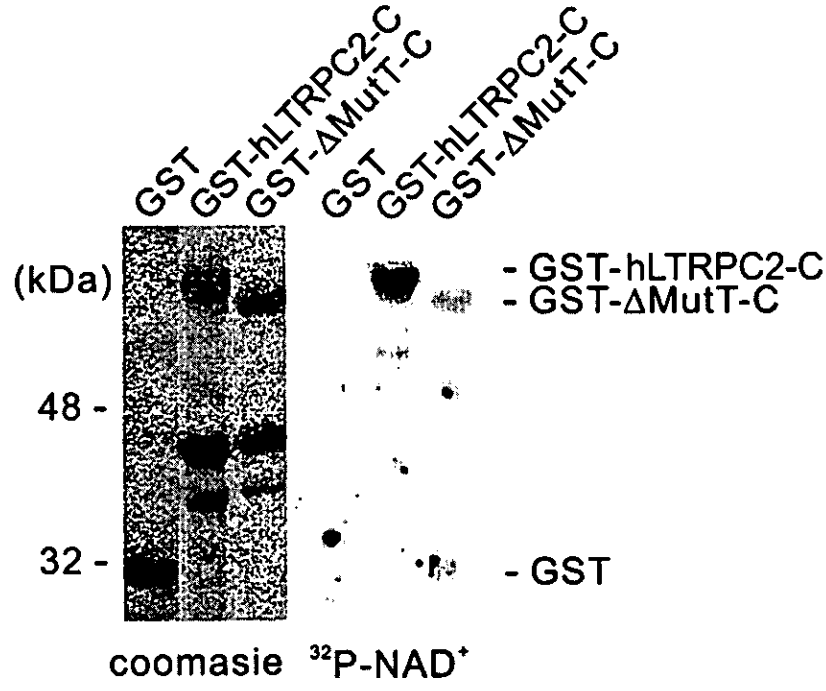
GST
GST-hLTRPC2-C
GST-ΔMutT-C
GST
GST-hLTRPC2-C
GST-ΔMutT-C
(kDa)
48 -
32 -
- GST-hLTRPC2-C
- GST-ΔMutT-C
- GST
coomasie
32P-NAD+

Figure 13 β-NAD^+-binding assay.

Total proteins from *E. coli* expressing the GST protein (GST), and the GST fusion proteins for the intact (GST-hLTRPC2-C) and MutT-deleted hLTRPC2 C-terminus (GST-ΔMutT-C) were fractionated by 12.5% SDS-polyacrylamide gel (equal amount of GST proteins were applied), and stained with coomasie brilliant blue (left) or transferred to nitrocellulose membrane for subsequent binding experiment (right). The membrane was incubated with [^{32}P]-NAD^+, washed, and subjected to autoradiography.

Figure 14

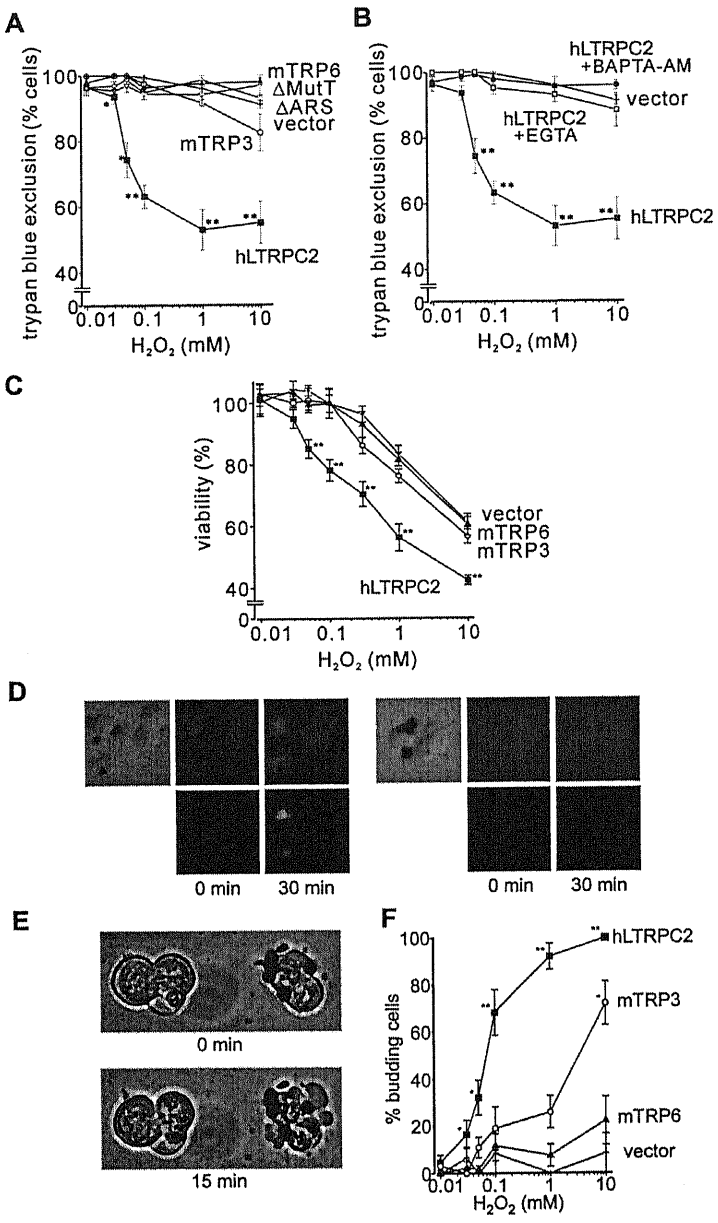
A
trypan blue exclusion (% cells)
100
80
60
40
0
mTRP6
ΔMutT
ΔARS
vector
mTRP3
hLTRPC2
0.01 0.1 1 10
H2O2 (mM)
B
trypan blue exclusion (% cells)
hLTRPC2
+BAPTA-AM
vector
hLTRPC2
+EGTA
hLTRPC2
H2O2 (mM)
C
viability (%)
vector
mTRP6
mTRP3
hLTRPC2
H2O2 (mM)
D
0 min
30 min
0 min
30 min
E
0 min
15 min
F
% budding cells
hLTRPC2
mTRP3
mTRP6
vector
H2O2 (mM)

Figure 14 LTRPC2 confers susceptibility to H_2O_2-induced death.

(A and B) Viability assessed by trypan blue exclusion. Cells transfected with hLTRPC2, ΔMutT, ΔARS, mTRP3, mTRP6, and vector were exposed to H_2O_2 in HBS, Ca^{2+}-free HBS, or BAPTA-AM-containing HBS solution for 20 min. Data points are the means ± S.E from 4 to 15 experiments.

(C) Viability assessed by the MTT assay. Cells transfected with hLTRPC2, mTRP3, mTRP6, and vector were exposed to H_2O_2 (1 h). The data were normalized by those measured in untreated cells. Each point from 6 to 17 observation.

(D) Simultaneous detection of H_2O_2-induced $[Ca^{2+}]_i$ changes (upper panels) and cell death (lower panels) by observing confocal fluorescent images of fluo-3 and PI, respectively, in hLTRPC2-transfected cells. Left panels, both $[Ca^{2+}]_i$ elevation and cell death were induced. Right panels, only $[Ca^{2+}]_i$ elevation was detected.

(E and F) H_2O_2-induced membrane budding. (E) Cells were incubated with H_2O_2 (100 μM) and Ca^{2+} (2 mM) for 15 min. Membrane budding was observed in LTRPC2-expressing cells attached with anti-CD8 antibody-coated beads (right), but not in CD8-negative cells (left). (F) Percentages of budding cells in hLTRPC2-, mTRP3-, mTRP6-, and vector-transfected cells after 15 min exposure to H_2O_2 (10 μM - 10 mM). * and ** indicate $P<0.05$ and $P<0.001$.

Figure 15

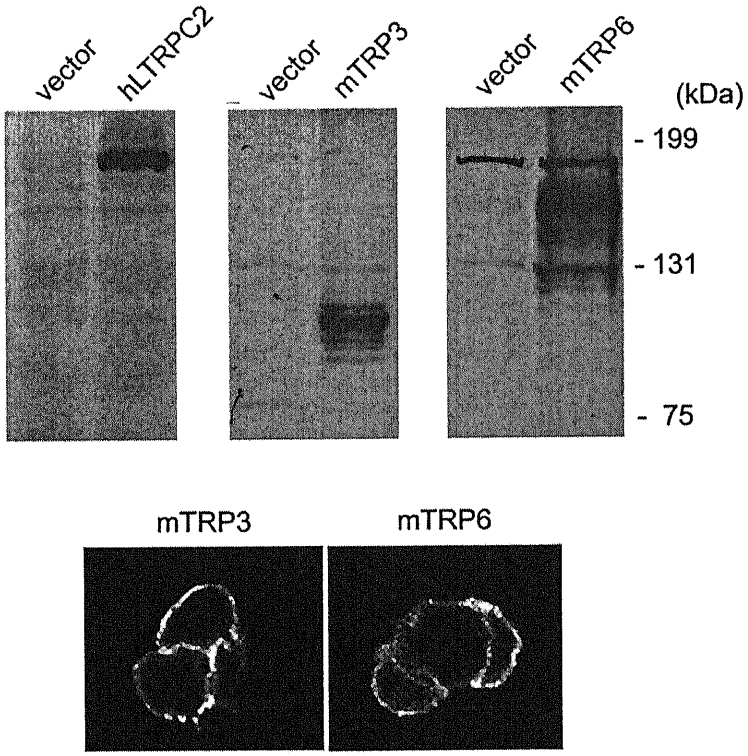
vector
hLTRPC2
vector
mTRP3
vector
mTRP6
(kDa)
- 199
- 131
- 75
mTRP3
mTRP6

Figure 15 Expression and membrane localization of mTRP3 and mTRP6 protein in transiently transfected HEK cells.

Western blot analysis and immunofluorescence staining of mTRP3 or mTRP6 proteins using the mTRP3-C1 or mTRP6-C1 antisera, respectively. To estimate the expression level of hLTRPC2, mTRP3 or mTRP6 in transfected HEK cells, the epitope peptides were used as standards in dot blot analysis (data not shown).

Figure 16

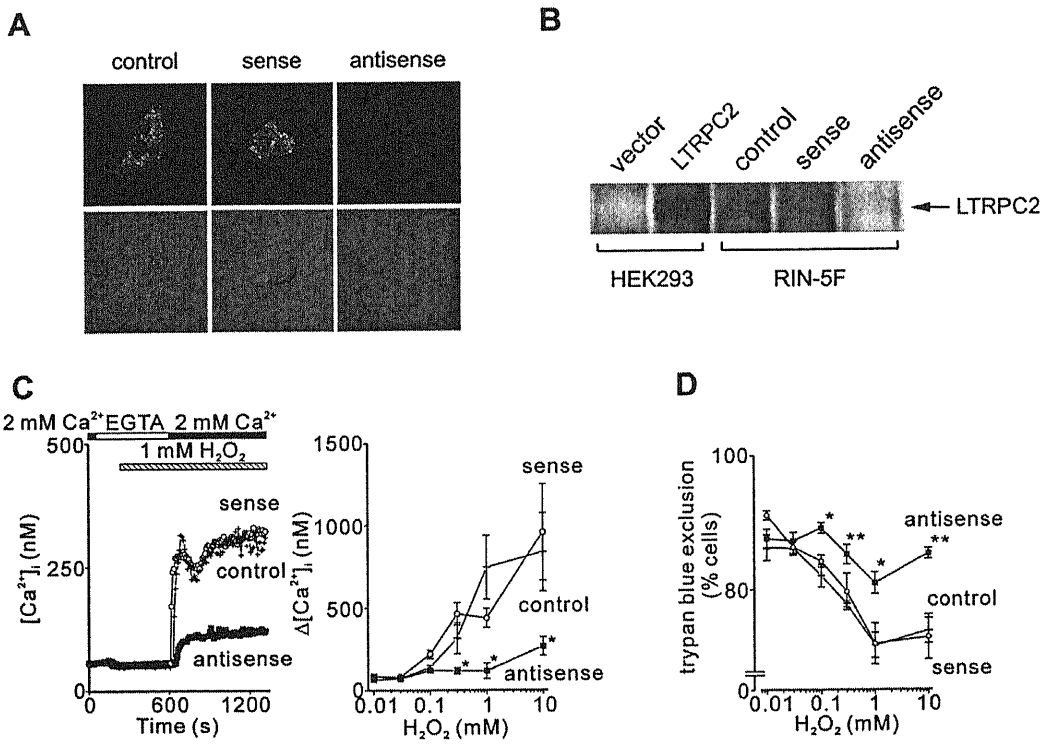
A
control
sense
antisense
B
vector
LTRPC2
control
sense
antisense
LTRPC2
HEK293
RIN-5F
C
2 mM Ca2+ EGTA 2 mM Ca2+
1 mM H2O2
sense
control
antisense
[Ca2+]i (nM)
Time (s)
Δ[Ca2+]i (nM)
H2O2 (mM)
D
trypan blue exclusion (% cells)
antisense
control
sense
H2O2 (mM)

Figure 16 Ca^{2+} influx and cell death mediated by 'native' LTRPC2 in response to hydrogen peroxide.

(A and B) LTRPC2 protein in rat insulinoma RIN-5F cells. (A) Confocal immunoimages of LTRPC2 (upper panels) and the corresponding DIC images of differential interference contrast (lower panels) in control (left) and sense oligonucleotide- (middle) or antisense oligonucleotide-treated RIN-5F cells (right). (B) Western blot analysis of LTRPC2 expression in RIN-5F and hLTRPC2-transfected HEK cells.

(C) Left, Ca^{2+} entry induced in LTRPC2 oligonucleotide-treated and control RIN-5F cells, after 6 min exposure to 1 mM H_2O_2 in the absence of external Ca^{2+}. Right, the maximum H_2O_2-induced $[Ca^{2+}]_i$ rises due to Ca^{2+} entry. * indicates $P<0.05$ compared with control cells.

(D) Viability assessed by trypan blue exclusion during exposure to H_2O_2 in LTRPC2 sense or antisense-treated and control RIN-5F cells. * and ** indicate $P<0.05$ and $P<0.001$, respectively.

Figure 17

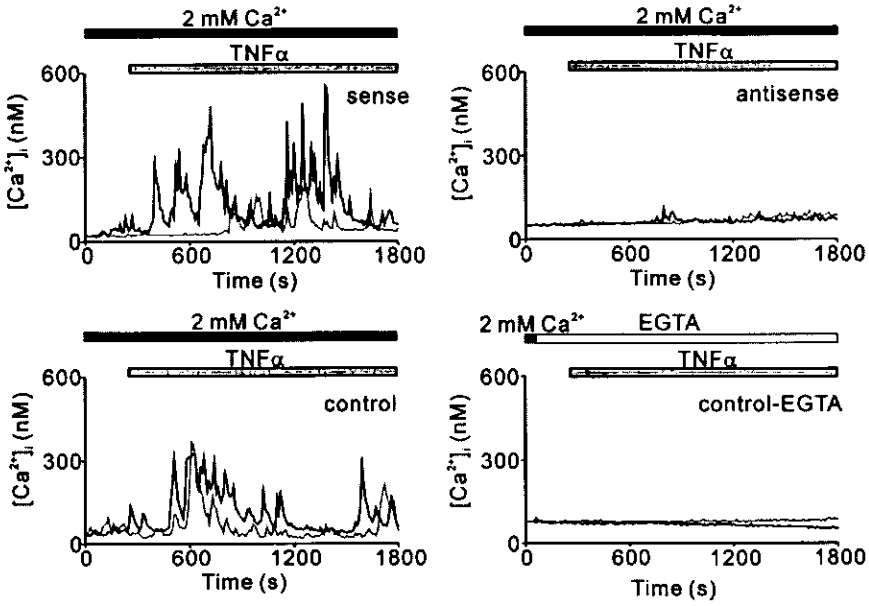
2 mM Ca2+
TNFα
sense
antisense
control
control-EGTA
EGTA
[Ca2+]i (nM)
600
300
0
0
600
1200
1800
Time (s)

Figure 17 LTRPC2 antisense ablates external Ca^{2+}-dependent $[Ca^{2+}]_i$ oscillations induced by TNFα in RIN-5F cells

Effects of antisense or sense treatment on oscillatory $[Ca^{2+}]_i$ responses induced by TNFα (1 μg/ml) in RIN-5F cells. Effect of co-incubation with EGTA is also shown.

Figure 18

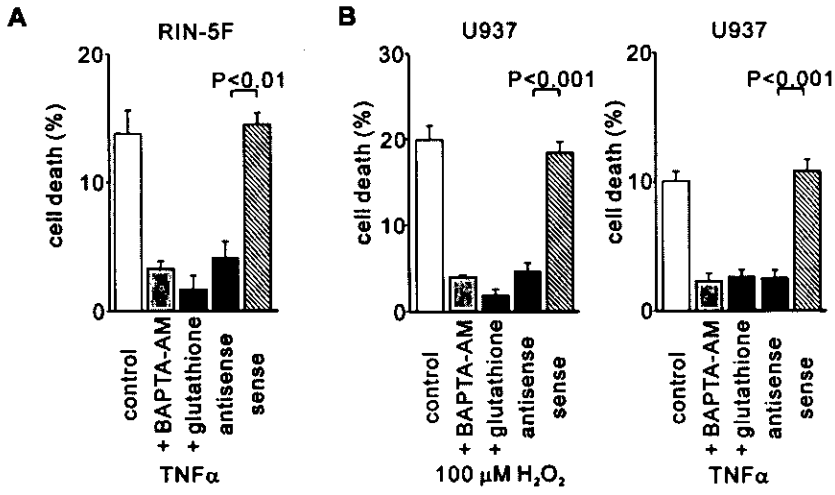
A
RIN-5F
cell death (%)
P<0.01
control
+ BAPTA-AM
+ glutathione
antisense
sense
TNFα
B
U937
cell death (%)
P<0.001
control
+ BAPTA-AM
+ glutathione
antisense
sense
100 μM H2O2
U937
cell death (%)
P<0.001
control
+ BAPTA-AM
+ glutathione
antisense
sense
TNFα

Figure 18 LTRPC2 antisense suppressed TNFα- and H_2O_2-induced cell death in RIN-5F or U937 cells

Effects of antisense or sense treatment, and of BAPTA-AM or glutathione on cell death induced by TNFα and H_2O_2 in RIN-5F (A) or U937 (B) cells. Percentages of cells that showed impaired trypan blue exclusion are indicated.

Figure 19

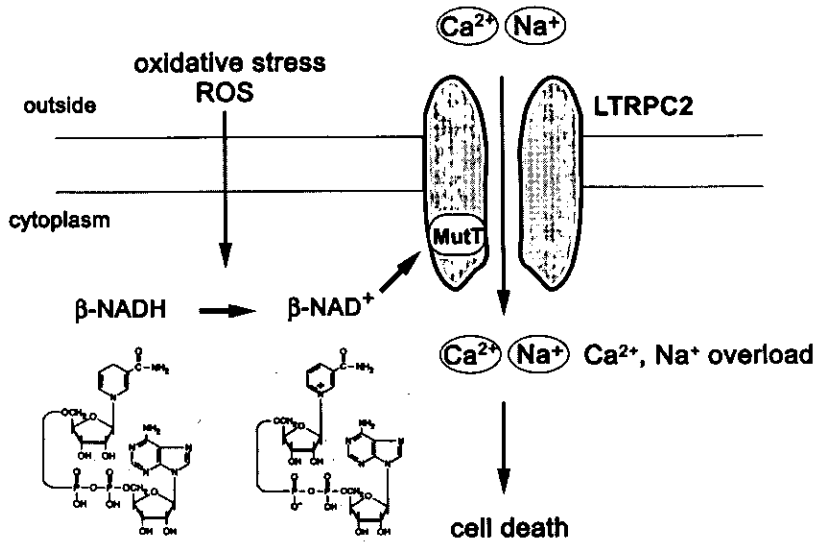
Ca2+ Na+
oxidative stress
ROS
outside
LTRPC2
cytoplasm
MutT
β-NADH
β-NAD+
Ca2+ Na+ Ca2+, Na+ overload
cell death

Figure 19. Schematic overview of postulated mechanism for LTRPC2 induced cell death signaling.

In response to the intracellular redox status modifiers, $NAD(P)^+/NAD(P)H$ is increased, and direct action of β-NAD^+ through the MutT motif is responsible for the activation of LTRPC2 channels. Then, hyperactivated LTRPC2 channel leads to $[Ca^{2+}]_i$ dysregulation, Na^+ overload and finally cell death.

ACKNOWLEDGMENTS

I should like to express my sincere gratefulness to Professor Yasuo Mori, Department of Molecular and Cellular Physiology, Center for Integrative Bioscience, the Graduate University of Advanced Studies and National Institute for Physiological Sciences, who showed me the essence of research work via supervising the present study.

I am deeply grateful to Professor Keiji Imoto, Department of Physiological Sciences, the Graduate University of Advanced Studies and Department of Information Physiology, National Institute for Physiological Sciences.

I am also deeply grateful to Professor Hiroshi Takeshima, Tohoku University Faculty of Medicine, in generating the LTRPC2 knockout mice.

I am also deeply grateful to Professor Yasunobu Okada and Dr. Emi Maeno, Department of Physiological Sciences, the Graduate University of Advanced Studies and Department of Cell Physiology, National Institute for Physiological Sciences, Dr. Minoru Wakamori, Kagoshima University, Faculty of Medicine, Dr. Shunichi Shimizu and Dr. Masakazu Ishii, Showa University, School of Pharmaceutical Sciences, Dr. Hitoshi Kurose, University of Tokyo, Graduate School of Pharmaceutical Sciences, Dr. Motohiro Nishida, Center for Integrative Bioscience.

I would also like to express special thanks to Ms. Emiko Mori, Ms. Kumiko Saito, Ms. Naomi Sekiguchi, Ms. Ai Nishihashi, and all other members of our laboratory. Without their help, it would have been much more difficult to accomplish this work.

Many thanks to my parents and brother, who have supported me to complete this thesis.

February 2002

Yuji Hara